Journal of Alloys and Compounds 932 (2023) 167611

Contents lists available at ScienceDirect

Journal of Alloys and Compounds

journal homepage: www.elsevier.com/locate/jalcom

Review

A review of microstructure control and mechanical performance optimization of γ-TiAl alloys

Runrun Xu [a], Miaoquan Li [b], Yonghao Zhao [a,*]

[a] Nano and Heterogeneous Materials Center, School of Materials Science and Engineering, Nanjing University of Science and Technology, Nanjing 210094, Jiangsu, PR China
[b] School of Materials Science and Engineering, Northwestern Polytechnical University, Xi'an 710072, Shaanxi, PR China

ARTICLE INFO

Article history:
Received 20 August 2022
Received in revised form 9 October 2022
Accepted 14 October 2022
Available online 17 October 2022

Keywords:
γ-TiAl alloys
Microstructure
Texture
Creep
Fatigue
Tribology

ABSTRACT

Upgrading and developing metallic materials are bases for improving the performance of aircraft. As one of the new structural metallic materials used in aerospace, lightweight and high-strength γ-TiAl alloys have been successfully used as high-risk structural parts in aircraft engines. Nonetheless, intrinsic embrittlement is the main factor limiting applications of γ-TiAl alloys. To further enlarge the application fields of γ-TiAl alloys, it is urgent to improve mechanical properties, like strength and ductility. This paper first introduces phase constituents and precipitates of γ-TiAl alloys, summarizes microstructure control measures of γ-TiAl alloys, and presents texture evolutions of γ-TiAl alloys. Then, based on four strength mechanisms, this review paper summarizes factors influencing mechanical properties of γ-TiAl alloys during compression, tension, creep and fatigue as well as tribology tests. It also includes the fracture mechanisms of γ-TiAl alloys. Finally, this paper proposes some future development directions for studying γ-TiAl alloys, like screening chemical compositions via machine learning technology, and developing microstructure evaluation software.

Contents

* Corresponding author.
E-mail address: yhzhao@njust.edu.cn (Y. Zhao).

https://doi.org/10.1016/j.jallcom.2022.167611
0925-8388/

1. Introduction

The development of human society is inseparable from metallic materials application. The use of bronze wares significantly promotes the development of ancient China's economy, culture (like Square vessel with four rams, in Fig. 1a) and military, giving impetus to the social progress of panhuman. Currently, metallic materials and their products have been widely used as essential tools in people's daily life and travel (like kettle and car). More importantly, metallic materials play crucial roles in biomedicine, electronic communication, transportation and aerospace fields, like aero engine (Fig. 1b) and Mars probe (Fig. 1c) [1,2].

Metallic materials can be divided into two categories by the dividing line with a density of 5 g·cm^{-3} [3]. The former are lightweight metallic materials, like aluminum, magnesium and titanium alloys. The latter are heavy metallic materials, like iron and steel, copper alloys and nickel-based superalloys. The strength and heat resistance of metallic materials are usually proportional to their density range. Therefore, the service performances and temperature of lightweight metallic materials are relatively low compared with those of heavy metallic materials and need to be further improved. The ultimate strength of aluminum alloys is often smaller than 650 MPa [4]. The ultimate strength and service temperature of titanium alloys are 1000 MPa (for TC21, [5,6]) and 600 ℃ (for Ti600), respectively. Therefore, titanium alloys are widely used in aviation industry, including landing gears, fan blades and other aircraft components far away from high-temperature region. In some aircraft, the usage of titanium alloys is as high as 50% [7]. However, the service performances and temperature of conventional lightweight metallic materials have gradually reached their limit recently, because the requirements dramatically increase for maneuverability and transportation capacity of aircraft.

Heavy materials, such as steel and nickel-based superalloys, are widely used in the aviation industry because of high service performances and temperature. For example, nickel-based superalloys are frequently used as components near high-temperature region of aero engines, such as turbine disks and low-pressure turbine (LPT) blades. However, the weight of nickel-based superalloys components is about 40%– 60% total weight of aero engines, which seriously impedes improvements in maneuverability and transportation capacity of aircraft. Thus, it is necessary to develop advanced metallic materials with lightweight and high service temperatures.

γ-TiAl alloys are titanium aluminides with the Al content of 42–49 at.% (atomic percent), which are considered as important substitutes for titanium alloys and nickel-based superalloys in aero engines. γ-TiAl alloys exhibit low density (~4 g·cm^{-3}), high service temperature (650–850 ℃), high specific strength, excellent creep and oxidation resistance. Besides, much attention has also been paid to poly-synthetically twinned TiAl (PST-TiAl) single crystal with a service temperature up to 900 ℃ [8]. The PST-TiAl single crystal with controlled lamellar orientations was prepared by directional solidification. It presents the elongation to failure of ~6.9% at room temperature, about triple that of polycrystalline γ-TiAl alloys, and an ultimate strength at room temperature of about 978 MPa, comparable to that (≥1016 MPa, [9]) of nickel-based superalloys. Due to remarkable advantages, γ-TiAl alloys have been commercially utilized in aero engines to partially replace Ni-based superalloys in the temperature range of 600–800 ℃ [10]. And the weight of GEnx engines was reduced by 200 pounds after equipping Ti-48Al-2 Nb-2Cr (termed as 4822 alloy) LPT blades. Nevertheless, the relative brittleness remains the Achilles' heel of γ-TiAl alloys, and limits the wider application in aerospace that requires safety and reliability without any catastrophic failure. In addition, the service temperature of γ-TiAl alloys also needs to be further raised to replace more Ni-based superalloys components in aero engines. Therefore, it is important to optimize mechanical properties, like ductility, strength and service temperature of γ-TiAl alloys via tailoring their microstructures [11].

Considering the relationship between microstructure and performance, this paper mainly summarizes recent study on microstructure control and mechanical properties optimization of polycrystalline γ-TiAl alloys. Besides, research progress on the tribological property and fracture mechanisms of polycrystalline γ-TiAl alloys are also reviewed.

2. Microstructure

2.1. Phase constituents

γ, α_2 and β_0 phases are main phase constituents of γ-TiAl alloys. γ phase (TiAl) has an $L1_0$ tetragonal structure with the *c* axis slightly larger than the *a* axis. Wang et al. [12] found that the *c*/*a* ratio of γ phase increases from 1.014 to 1.021 as the Al content increases from 42 at.% to 51 at.%. Fang et al. [13] claimed that adding Ta reduces the

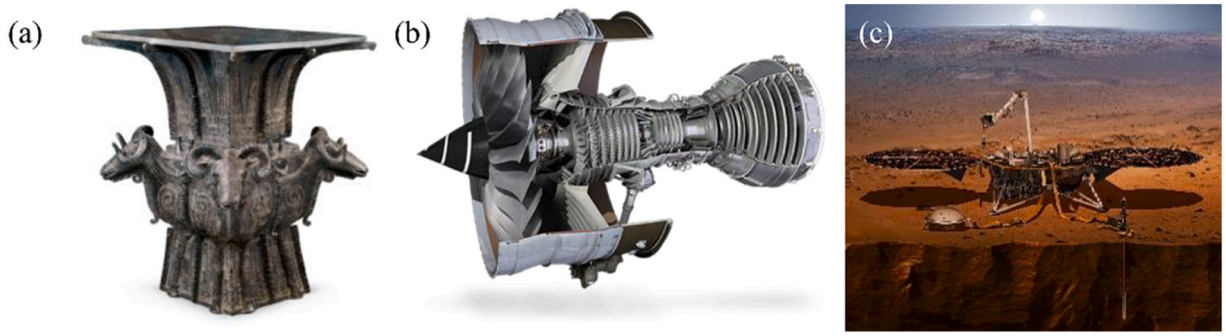

Fig. 1. (a) Square vessel (fang zun) with four rams (National Museum of China); (b) Trent XWB aero engine (Rolls-Royce), (c) Insight Mars lander (NASA).

Table 1
Lattice parameters and chemical compositions of phase constituents in γ-TiAl alloys.

Phase	Lattice parameters /Å	Compositions /at.%				Ref.
		Ti	Al	Nb	Cr	
γ	c= 4.05, a= 4.02	43.12	47.85	5.38	2.17	[14]
α_2	c= 4.64, a= 5.76	61.58	31.60	2.12	2.09	[14,17]
β_0	a=c= 3.31	51.09	36.08	5.81	6.21	[14,18]
ω	a= 4.56, c= 5.65	48.47	22.50	27.17	—	[19,20]
O	a= 5.92, b= 9.80, c= 4.67	54	37	9	—	[21]

value of *a* axis, but increases the value of *c* axis and the *c*/*a* ratio of γ phase. Besides, for γ-TiAl alloys prepared by using directional solidification technique, the *c*/*a* ratio of γ phase decreases from 1.012 to 1.002 with the increasing of growth rate from 0.2 mm·min^{-1} to 1.0 mm·min^{-1} [14]. Meanwhile, both the lattice parameters and chemical compositions of γ, α_2 and β_0 phases are also altered with the growth rate for directionally solidified γ-TiAl alloys, as exhibited in Table 1. α_2 phase (Ti_3Al) presents a $D0_{19}$ hexagonal structure, and α_2 lamellae show Blackburn orientation relationships of $\{111\}\gamma||(0001)\alpha_2$ and $<1\bar{1}0]\gamma|| < 11\bar{2}0 > \alpha_2$ with γ lamellae. Additionally, the value of *a* axis slightly decreases, while the value of *c* axis and the *c*/*a* ratio of α_2 phase increase after adding Ta element [13]. β_0 phase has a body-centered cubic structure, and is rich in Cr and Mo elements [15]. Although β_0 phase significantly increases after adding Nb element, the Nb enrichment in β_0 phase is hard to figure out due to the sluggish diffusion of Nb element. Sometimes β_0 phase exists special orientation relationships of $\{111\}\gamma||(0001)\alpha_2||(110)\beta_0$ and $<1\bar{1}0]\gamma|| < 11\bar{2}0 > \alpha_2|| < 111 > \beta_0$ to γ and α_2 phases [16].

Aside from above phase constituents, γ-TiAl alloys also contain some other minor phase constituents, like ω, ω_0, O, τ_2, Ti_2Al and B19 phases [22,23]. ω phase ($Ti_6Al_6Nb_4$) has a $D8_8$ hexagonal structure, and the lattice parameters and chemical compositions are presented in Table 1. ω phase is mainly precipitated from β_0 phase with the orientation relationships of $\{10\bar{1}0\}\omega||\{110\}\beta_0$ and $<0001 > \omega|| < 1\bar{1}1 > \beta_0$ [24,25]. ω_0 phase (Ti_4Al_3Nb) has a $B8_2$ structure, with the chemical composition of Ti-31.37Al-18.2 Nb-0.73 W (at.%) [20]. ω_0 phase is formed in β_0 or α_2 phase, with the orientation relationships of $(1120)\omega_0||(0001)\alpha_2$ and $[0001]\omega_0||[1120]\alpha_2$ to α_2 phase [26–28]. Particularly, the $\alpha_2 \rightarrow \omega_0$ phase transformation is tightly linked to Nb element diffusion [29]. O phase (Ti_2AlNb) has an orthorhombic structure, and keeps the orientation relationships of $\{001\}O||(0001)\alpha_2$ and $<110 > O|| < 11\bar{2}0 > \alpha_2$ to α_2 phase [30]. O phase is mainly generated from α_2 phase, or precipitated from α_2' martensitic phase [21,31]. The precipitated O phase increases the nano Vickers hardness of α_2/γ lamellar colonies up to 13.78% [32]. Rackel et al. [33] found that the O phase is prone to precipitate when γ-TiAl alloys with the Al contents of 46–47 at.% were heat-treated at 550 ℃. Besides, they found that the formation of O phase is induced by adding Nb, Mo, Ta and V elements, whereas unaffected by adding B and C elements. Dai et al. [29] reported that Nb element is the primary factor governing $\alpha_2 \rightarrow$O phase transformation. Furthermore, the addition of Fe element would introduce τ_2 phase with the chemical composition of Ti-38.16Al-22.8Fe-2.25 Nb (at.%) in γ-TiAl alloy [34].

Ti_2Al and B19 phases are metastable phases in γ-TiAl alloys. During high-pressure torsion of γ-TiAl alloys, α_2 phase is transformed into γ phase through Ti_2Al and $Ti_{1.4}Al$ intermediate phases, as shown in Fig. 2a-b. The crystal structure of Ti_2Al phase is the same as that of α_2 phase, and the crystal structure of $Ti_{1.4}Al$ is the same as that of γ phase [35]. In addition, Ti_2Al phase might be precipitated on α_2/γ lamellar interface with the orientation relationships of and to α_2 and γ lamellae [22]. B19 phase has an orthorhombic structure, which is formed in the temperature range of 600–700 ℃. It often acts as an intermediate phase when supersaturated α_2 phase decomposed into α_2 and γ phases, or β_0 phase transformed into O phase [36,37]. In some cases, B19 phase is precipitated from γ lamellae with the orientation relationship of during room temperature tension of Ti-45.6Al-7.7 Nb-0.2 C (Fig. 2c) [38]. Notably, the authors also observed a similar γ→B19 phase transformation during heat treatment of lamellar 4822 alloy.

2.2. Precipitates

Except for various phase constituents, γ-TiAl alloys also exist some precipitates, like borides, carbides and silicides. TiB exhibits B27 and B_f orthorhombic structures. According to previous research [39,40], various elements play vital roles in the formations of B27 and B_f TiB. B27 TiB is promoted by Nb and Ta elements, but inhibited by Mn element. Yet B_f TiB is accelerated by Ta and Hf elements, but impelled by Mn and Nb elements. TiB_2 shows a C32 hexagonal structure, and sometimes presents special orientation relationships (and) to β_0 phase [41]. TiB_2 promotes the α_2 and γ lamellae nucleation and then refines α_2/γ lamellar colonies [42,43]. More precisely, TiB_2 would appear in two kinds of morphologies: flake and block (Fig. 3a-b), and only the block TiB_2 has a large impact on the lamellar spacing of α_2/γ lamellar colonies [44].

There are two kinds of carbides in γ-TiAl alloys: H-Ti_2AlC with a hexagonal structure and P-Ti_3AlC with an E21 cubic structure. Wang et al. [45] found that the orientation relationships between H-Ti_2AlC and γ phase are $<11\bar{2}0 > H|| < 101]\gamma$ and $(0001)H||\{111\}\gamma$. And the orientation relationships between P-Ti_3AlC and γ phase are $<100 > P|| < 100]\gamma$and $(010)P||(010)\gamma$. The volume fraction of H-

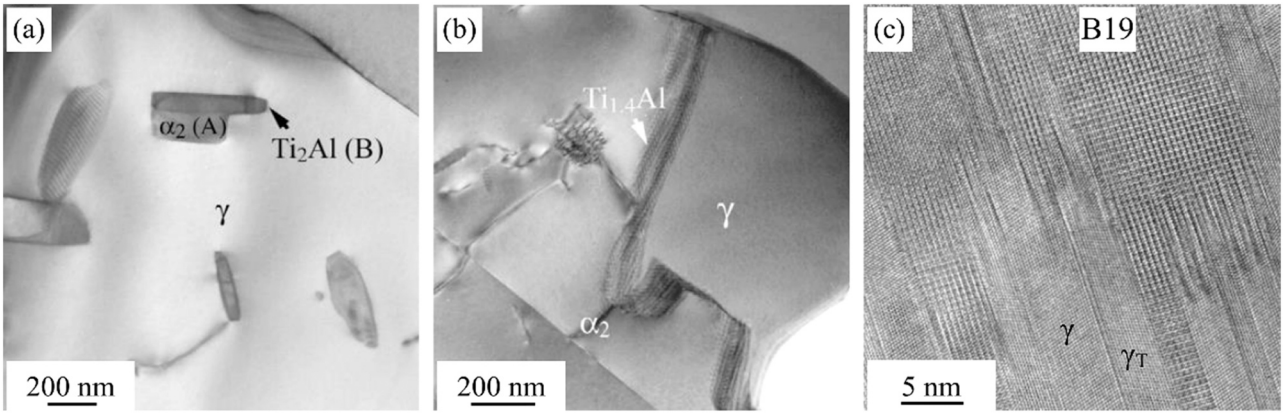

Fig. 2. (a)-(b)TEM bright-field images of (a) Ti_2Al and (b) $Ti_{1.4}Al$ metastable phases [35], (c) HRTEM image of B19 phase in α_2/γ lamellar colonies [38].

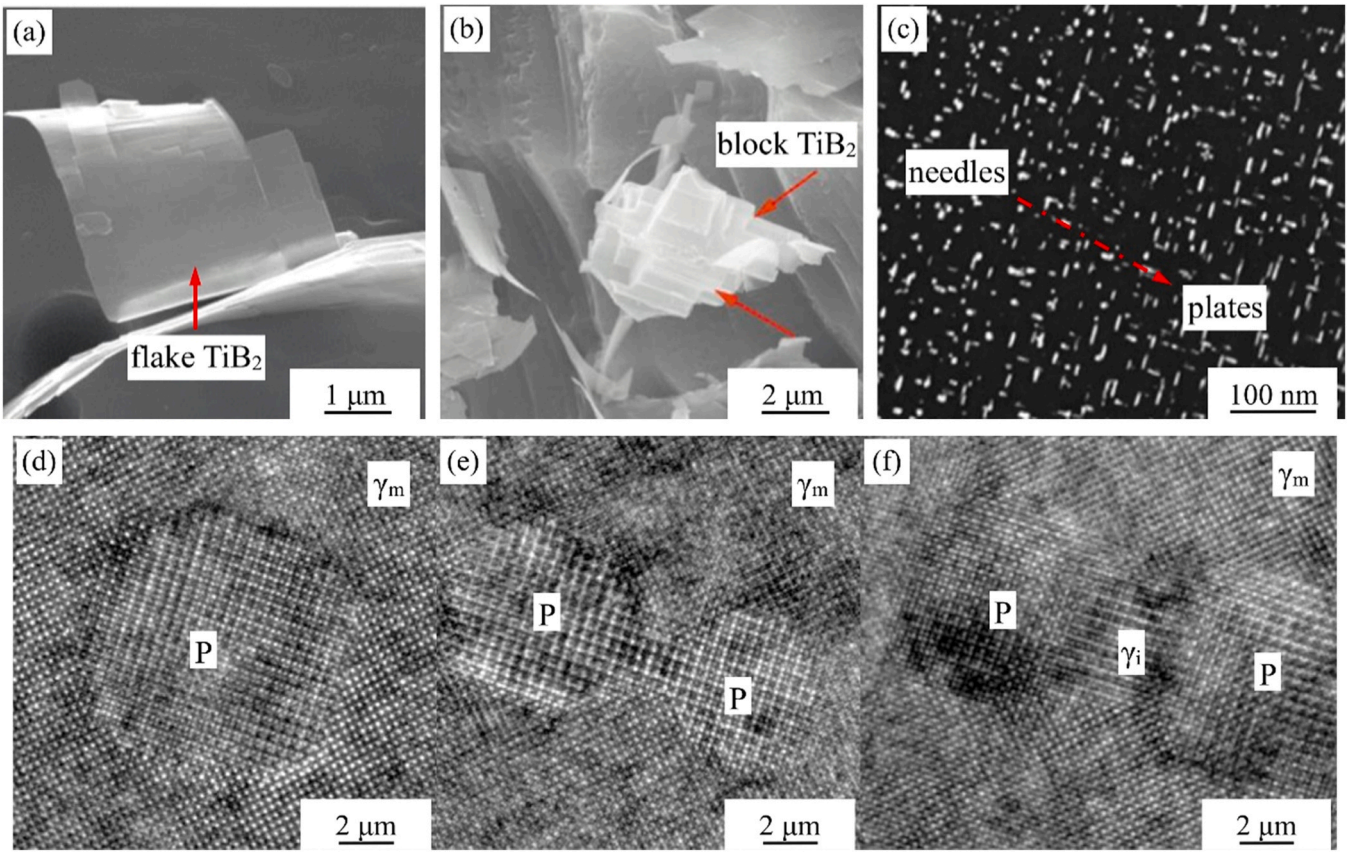

Fig. 3. (a)-(b) SEM images for: (a) flake and (b) block TiB_2 [42]. (c) Bright-field TEM image of P-Ti_3AlC, (d)-(f) HRTEM images of P-Ti_3AlC: (d) needle shape, (e) dumbbell shape, (f) sub-particles [47].

Ti_2AlC increases with the increasing of annealing time, while the volume fraction of P-Ti_3AlC decreases by splitting. Similar rules also can be found as the contents of Al and C elements increase. Moreover, increasing the creep pressure facilitates the formation of H-Ti_2AlC on α_2/γ lamellar interfaces [46]. Fig. 3c-f reveals the splitting process of P-Ti_3AlC when γ-TiAl alloy annealed at 800 ℃. The needle P-Ti_3AlC (Fig. 3d) initially transforms into plates (Fig. 3c), then changes to dumbbell shape via P/γ phase interface bulging (Fig. 3e), and finally splits into sub-particles (Fig. 3 f) [47].

As the common silicide, ζ-Ti_5Si_3 has a $D8_8$ hexagonal structure, and acts as one of the strengthening phases in γ-TiAl alloys. Klein et al. [48] found that ζ-Ti_5Si_3 is mainly distributed in β_0 phase via ab *initio* calculations. Howbeit, ζ-Ti_5Si_3 shows orientation relationships of $(0110)\zeta\| < 011]\gamma$ and $(0002)\zeta\| < 233]\gamma$ to γ phase [49]. During directional solidifying of γ-TiAl alloy, ζ-Ti_5Si_3 morphology would gradually change from short rods to long strips along the growth direction [50].

2.3. Typical microstructures

Both γ and α phases in γ-TiAl alloys are presented in two forms: lamellae and grains. According to the volume fraction of α_2/γ lamellar colonies and γ grains, γ-TiAl alloys can be divided into four typical categories: near gamma, duplex, nearly lamellar and fully lamellar structure (Fig. 4a-d). Fig. 4e-f presents tensile stress-strain curves of γ-TiAl alloys with four typical microstructures. Whether tested at room temperature or 700 ℃, the elongation to failure of fully lamellar structure is minimum, followed by nearly lamellar and duplex structure, and that of near gamma structure is maximum, as exhibited in Fig. 4e-f. At a given strain, the tensile strength order of γ-TiAl alloys is just opposite to the order of elongation to failure. Apparently, the tensile strength of γ-TiAl alloys increases while the elongation to failure decreases as the volume fraction of α_2/γ lamellar colonies increases.

This phenomenon can be explained in the following. Compared to γ phase with tetragonal structure, α_2 phase with hexagonal structure is hard to deform for lacking independent dislocation systems. Therefore, from the perspective of crystallographic structure, the ductility of α_2/γ lamellar colonies is often lower than that of γ grains at given orientations. Besides, various lamellar interfaces, like γ/γ twin interfaces can be found in a single α_2/γ lamellar colony. These lamellar interfaces are effective barriers for dislocation slip and twinning, and thus would induce stress concentrations at lamellar interfaces. Hence for the given grain sizes, the ductility of α_2/γ lamellar colonies is generally lower than that of γ grains. Moreover, the mechanical properties of α_2/γ lamellar colonies are dependent on lamellar orientations (the intersection angle between lamellar interface and loading direction). PST-TiAl single crystal is a single α_2/γ lamellar colony. Yao et al. [52] and Kim et al. [53] confirmed that the yield strength and elongation to failure of PST-TiAl single crystal at room temperature are sensitive to lamellar orientations, as shown in Fig. 5a-b. Imayev et al. [54] found that the compressive properties of PST-TiAl single crystal at high temperature are also tightly linked to lamellar orientations, as shown in Fig. 5c. α_2/γ lamellar colonies with orientation angles closing to 0 deg. and/or 90 deg. are hard for plastic deformation, and thus present poor ductility. However, α_2/γ lamellar colonies with orientations ranging from 0 deg. to 90 deg. often coexist in polycrystalline γ-TiAl alloys. To a certain degree, the occurrence of α_2/γ lamellar colonies would deteriorate the ductility but improve the strength of γ-TiAl alloys. For the above reasons, the ductility of γ-TiAl alloys decreases with the increase of α_2/γ lamellar colonies. Furthermore, Schwaighofer et al. [55] also confirmed that

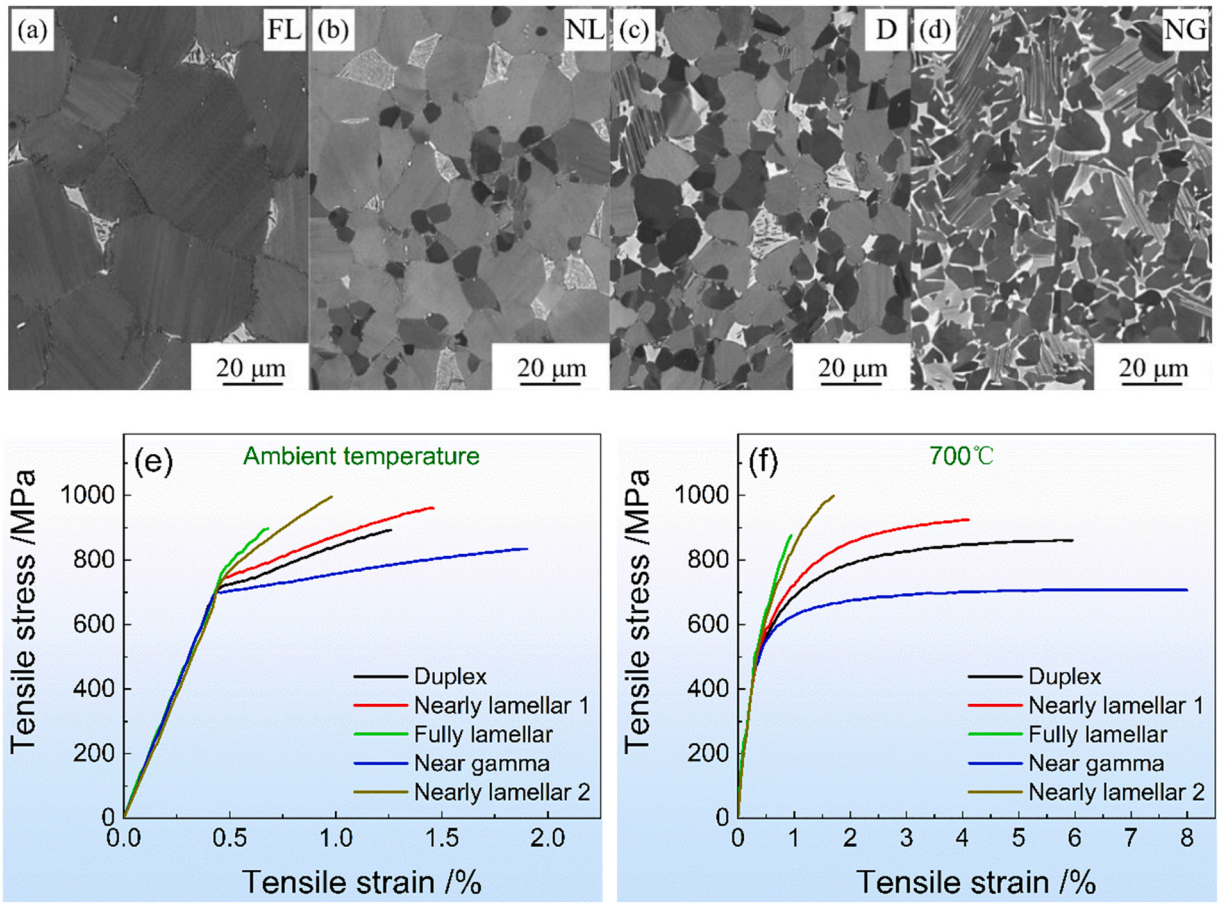

Fig. 4. Typical microstructures of γ-TiAl alloys: (a) fully lamellar, (b) nearly lamellar, (c) duplex, (d) near gamma structure. Tensile stress-strain curves of various γ-TiAl alloys tested at: (e) ambient temperature, (f) 700 ℃ [51].

the ductility at room temperature of TNM alloys decreases with the increase of α_2/γ lamellar colonies or decrease of γ grains.

To achieve a better combination between strength and toughness, the microstructure of γ-TiAl alloys was controlled via alternating microstructure morphologies, phase constituents and precipitates. Fully lamellar γ-TiAl alloy including minor TiB_2, ζ-Ti_5Si_3 and P-Ti_3AlC was fabricated via chemical composition design and heat treatment process optimization, and this γ-TiAl alloy possesses low yield strength, better creep resistance and high service temperature up to 850 ℃ [56]. When γ-TiAl alloy annealed at 800–900 ℃, α_2/γ lamellar colonies would be transformed into ($\alpha_2+\beta_0+\gamma$) pearlitic-like structure (termed as “cellular reaction”) [55]. Prolonging the annealing time, α_2/γ lamellar colonies are gradually changed into ($\beta_0+\gamma$) pearlitic-like structure, resulting in two γ-TiAl alloys with new structures, as shown in Fig. 6a-b. Compared with fully lamellar structure, such new γ-TiAl alloys present a good combination of ultimate strength and elongation to failure at room temperature [57]. The ultimate strength is about 977.61 MPa, close to that (978 MPa) of PST-TiAl [8]. And the elongation to failure is two times of that for γ-TiAl alloys with fully lamellar structure.

2.4. Microstructure control methods

2.4.1. Chemical composition design

Up to now, intensive efforts have been paid for microstructure control of γ-TiAl alloys. The microstructure is sensitive to many factors, like chemical compositions and processing parameters. Hence identifying the effect of elements is the first task for chemical composition design, microstructure control and mechanical properties improvement of γ-TiAl alloys.

As the primary element of γ-TiAl alloys, Al element not only influences the solidification path and phase content, but also alternates the lamellar spacing of α_2/γ lamellar colonies. With regards to binary γ-TiAl alloys, minimum lamellar spacing is achieved (maximum number of lamellar interfaces is introduced) in γ-TiAl alloys with the Al content of 41.5 at.% [58]. Four lamellar interfaces can be found in α_2/γ lamellar colonies: α_2/γ lamellar interface, γ/γ pseudo twin interface, γ/γ rotational variants interface and γ/γ true twin interface. Xiang et al. [59] claimed that α_2/γ and γ/γ lamellar interfaces have a synergetic effect to improve the strength and plasticity of PST-TiAl single crystal, and the synergetic effect enhances by increasing the volume fraction of γ/γ lamellar interface. More specifically, the fracture toughness of PST-TiAl single crystal is promoted by increasing the volume fraction of γ/γ pseudo twin interface and γ/γ rotational variants interface [60].

The volume fraction of β_0 phase increases by adding Nb element into γ-TiAl alloys, and so does the service temperature of γ-TiAl alloys. Except for Nb element, adding Co [61], Cr [62], Gd [18,63], Mn [64,65], Mo [66], Ta [13,67], W [68], V [69], Y [70], Zr [71] and other metallic elements, or B, C and Si non-metallic elements, also can alternate the solidification path, microstructure parameters, and thus improve the strength and/or ductility of γ-TiAl alloys. If the content of non-metallic elements, like C element, is lower than their corresponding solid solidification limit, the non-metallic elements would distribute as interstitial atoms in phases of γ-TiAl alloys [72]. Otherwise, the non-metallic elements would distribute as precipitates in γ-TiAl alloys. Fang et al. [73] claimed that adding C

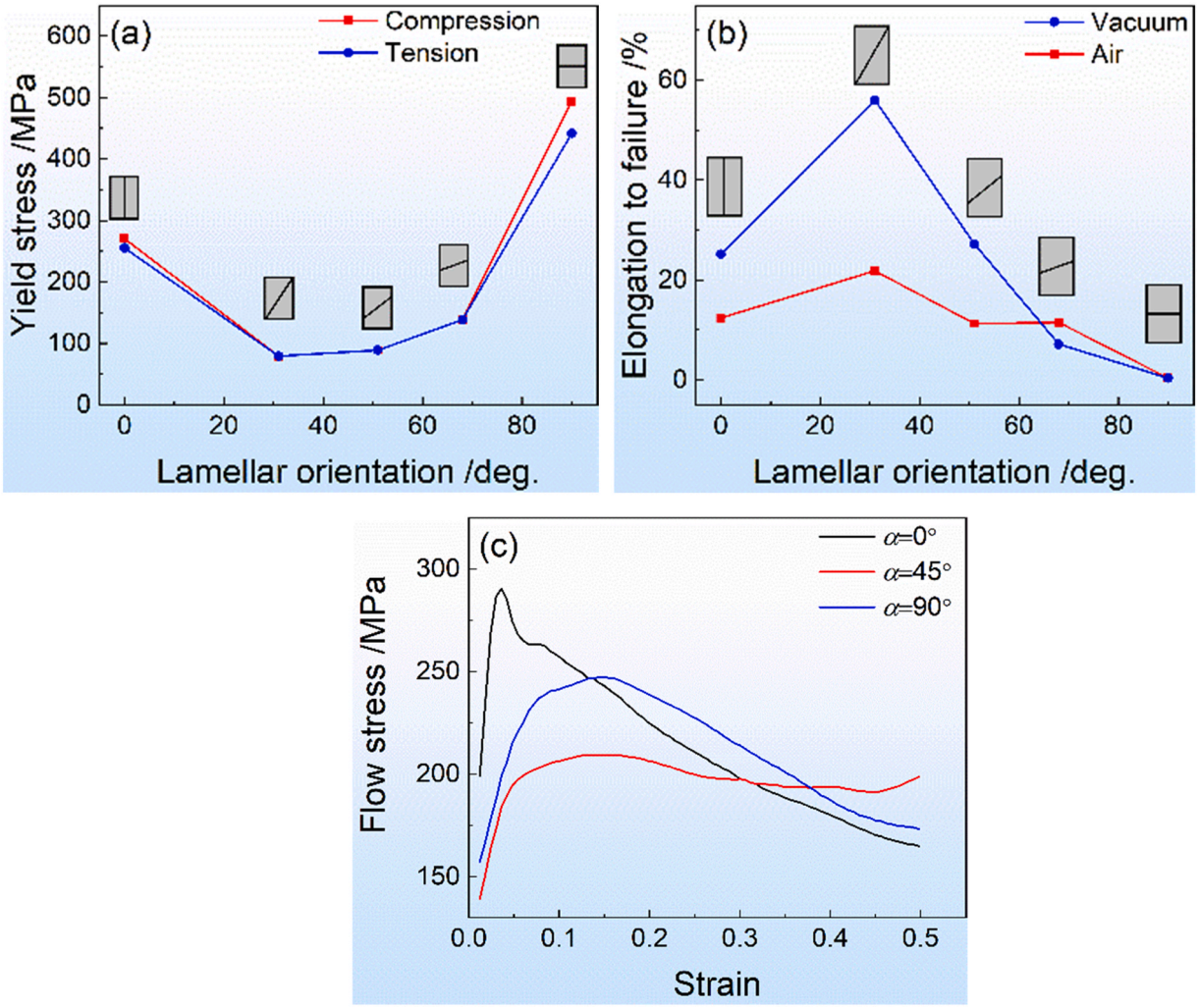

Fig. 5. The orientation dependence of (a) yield strength [53] and (b) elongation to failure of PST-TiAl single crystal [52]. (c) Flow stress-strain curves of PST-TiAl single crystal hot compressed at a deformation temperature of 1000 ℃ and strain rate of 0.001 s^{-1} [54].

element decreases the grain size and lamellar spacing of α_2/γ lamellar colonies, but simultaneously increases the volume fraction of β_0 phase whether C element is distributed as interstitial atoms or precipitates in γ-TiAl alloys.

2.4.2. Processing routes optimization

Processing routes, like post-heat treatments and plastic deformation, would affect the microstructure of γ-TiAl alloys [74]. Post-heat treatments eliminate the element segregation and solidification

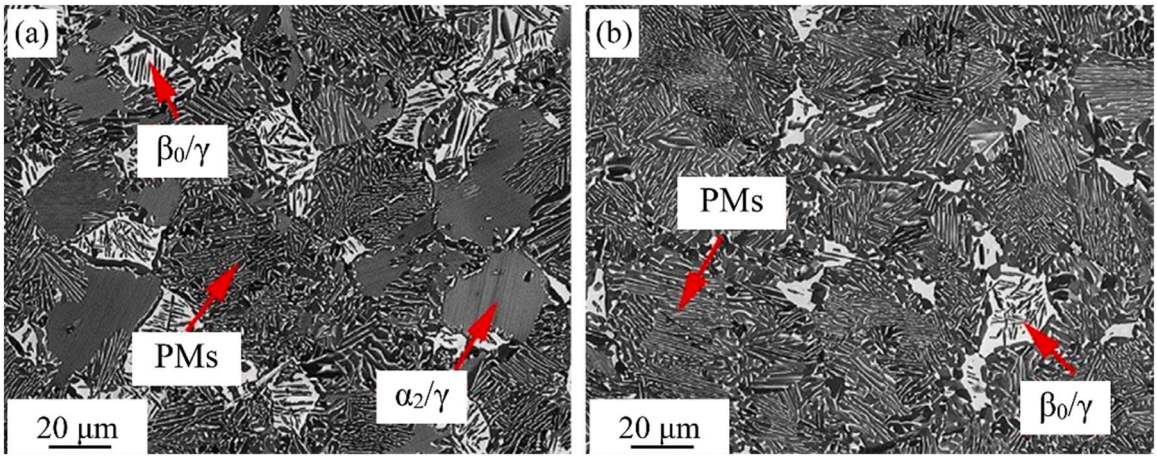

Fig. 6. New γ-TiAl alloys containing: (a) α_2/γ lamellar colonies and (β+γ) pearlite-like structure, (b) (β+γ) pearlite-like structure [57].

texture of γ-TiAl alloys [75]. Also, the cracking tendency is decreased. Besides, heat treatments may influence the phase content and grain size of γ-TiAl alloys [55]. Liu et al. [76] found that post-heat treatments of γ-TiAl alloys decreases the volume fraction of (β_0+γ) pearlitic-like structure and refine γ lamellae in α_2/γ lamellar colonies.

Hot deformation could remove the solidification textures and destroy coarse columnar grains in γ-TiAl ingot, achieving microstructure control and service performance improvement of γ-TiAl alloys. Xu et al. [77,78] previously found that both the phase content and microstructure parameters of isothermally compressed γ-TiAl alloys change with the change of deformation temperature, strain rate and strain due to the enhancement of dynamic recrystallization (DRX). As seen from Fig. 7a-b, DRX effect of α_2 grains heightens with the increasing of strain. Besides, with the increase of deformation temperature, the volume fraction of high angle grain boundary (HAGB) for γ grains increases (Fig. 7c-d), indicating the enhancement of DRX. So does the DRX of β_0 grains (Fig. 7e).

2.4.3. Other energy fields auxiliary

The microstructure control of γ-TiAl alloys is mainly achieved under thermal and/or force fields. In some cases, the microstructure control is carried out with the help of electrical, ultrasonic or plasma fields. Chen et al. [80] introduced pulse direct current into γ-TiAl alloy solidification process. Results showed that pulse direct current not only suppresses the formation of columnar grains and element segregation, but also decreases the grain size and lamellar spacing of α_2/γ lamellar colonies. Similar to electrical field, introducing ultrasonic field also eliminates solidification defects and refines the microstructure of γ-TiAl alloy ingot, yielding high compressive strength and relative compressibility [81]. Moreover, the microstructure of γ-TiAl alloys can be changed via Kr-ion irradiation [82]. Increasing the Kr-ion dose increases the size and content of stacking faults, but decreases the content of interstitial clusters in γ-TiAl alloy irradiated at room temperature [83].

2.4.4. Additive manufacturing

Unlike traditional manufacturing methods, additive manufacturing is a manufacturing route integrating material, structure and performance [2]. The route has attracted much attention due to high manufacturing efficiency, high material utilization rate and less-strict requirements for component shape [84,85]. For example, electron beam melting (EBM) has been utilized to fabricate 4822 alloy LPT blades, and reduces components amount from 300 to 7 in GE9x aero engines [86]. The compressive properties of γ-TiAl alloys components fabricated by laser-based additive manufacturing are close to or even higher than that of components fabricated by traditional manufacturing [87]. Hence additive manufacturing has been proved as an advanced approach to fabricating γ-TiAl alloys components.

Despite the above advantages, solidification cracking is a usual defect during additive manufacturing of γ-TiAl alloys, because the solidification is far from the equilibrium state [88]. Liquation cracking is also a common defect caused by grain boundaries segregation [89]. Wang et al. [90] found that cracking occurs in Nb-depletion regions and at α_2/β_0 phase interface during selective laser melting of 4822 alloy. To avoid the above-mentioned cracking, intensive efforts have been paid, like process optimization, chemical composition design and shape optimization of alloys powders [12,84,91,92]. Varying energy density can effectively control microstructure and increase tensile properties of γ-TiAl alloys fabricated by electron beam melting [93]. Besides, the LaB6 inoculation can effectively inhibit cracking during laser-based additive manufacturing of γ-TiAl alloys [87]. The microstructure of γ-TiAl alloys additive manufacturing components is also linked to chemical compositions [12,94], additive manufacturing routes and parameters [95], and post-heat treatments [96]. This part is briefly summarized below.

Chemical compositions, phase contents and mechanical properties of γ-TiAl alloys fabricated by EBM, are tightly linked to electron beam current and scanning speed, and the underlying cause is Al evaporation [97]. With the increasing of aging temperature from 700 ℃ to 900 ℃, the microstructure of γ-TiAl alloys fabricated via direct laser deposition changes from lamellar to near gamma structure. The formation of γ phase is connected to 6 H-type long periodic stacking ordered (LPSO) phase, and the formation of γ grains is relevant to 9R-type and 18R-type LPSO phases [98].

In essence, additive manufacturing is a processing technology combining rapid solidification and local remelting. Large differences of thermal field exist in surface and center areas of additive manufacturing components, which might help to fabricate γ-TiAl alloys with gradient structure. Fig. 8 shows the γ-TiAl alloys with gradient structure fabricated via laser remelting and post-heat treatment. As seen from Fig. 8, the surface and center regions exhibit duplex and near gamma structures, respectively. Except for common γ/γ interfaces, a special γ/γ interface with the orientation relationship of $<10\bar{1} > \gamma_1 \| < 411 > \gamma_2$ is also formed in α_2/γ lamellar colonies for γ-TiAl alloys prepared via gas tungsten arc welding [99]. Such the special γ/γ interface can absorb irradiation defects like sessile vacancy at room temperature, and suppress the formation of irradiation defects like stacking faults at high temperature. Therefore, the new γ/γ interface further enhances the damage tolerance of γ-TiAl alloys components during Kr-ion irradiation.

2.5. Texture

$L1_0$-type γ phase has an intrinsic anisotropy, making the microstructure and performance of γ phase differ with the orientation. Compared with γ grains, γ lamellae are more sensitive to anisotropy. For PST-TiAl single crystal, the compressive deformation and dynamic recrystallization behaviors vary with the orientation [54]. Also, the yield strength and elongation to failure are sensitive to the orientation whether PST-TiAl single crystal is tested at room temperature or high temperature [8]. So identifying texture evolutions during manufacturing, and then tailoring texture targeted to service performance are rather essential for precise manufacturing of γ-TiAl alloys.

According to the stress state, the texture in metallic materials can be divided into two types. The one is $<uvw>$ -denoted fiber texture after uniaxial deformations like compression, and the other is $\{hkl\}<uvw>$ -denoted sheet texture after multidirectional deformations like rolling. Both textures are reported in deformed γ-TiAl alloys. When γ-TiAl alloy is hot-forged in (α+β) phase field, $< 110 >$, $<11\bar{2}0>$ and $< 001 >$ fiber textures are formed in γ, α_2 and β_0 phases, respectively [101]. And the fiber texture intensity in γ phase is unaffected after long-time annealing below the $T_{\alpha\rightarrow\alpha2,\ \text{ordering}}$ transformation temperature. Hydrogenation treatment would weaken the $< 111 >$ fiber texture, but enhance $< 110 >$ and $< 320 >$ fiber textures in γ phase during isothermal compression [102]. The reason is that hydrogen promotes initial α_2/γ lamellar colonies decomposition and dynamic recrystallization. In most cases, the intensity of fiber texture in β_0 phase is quite weaker than that in γ and α_2 phases during uniaxial deformation, due to the excellent deformability and fast DRX rate of β_0 phase with cubic structure [79].

Sheet textures in hot-rolled γ-TiAl alloys are relatively complex, and may consist of two textures: deformation and recrystallization textures. Both textures are sensitive to rolling parameters. With the increase of rolling temperature, the DRX behavior improves. This might weaken the intensity of deformation texture and enhance that of recrystallization texture. When rolling temperature further increases from 1100 ℃ to 1200 ℃, the recrystallization texture in γ-TiAl alloy would be transformed into random textures [103]. As the

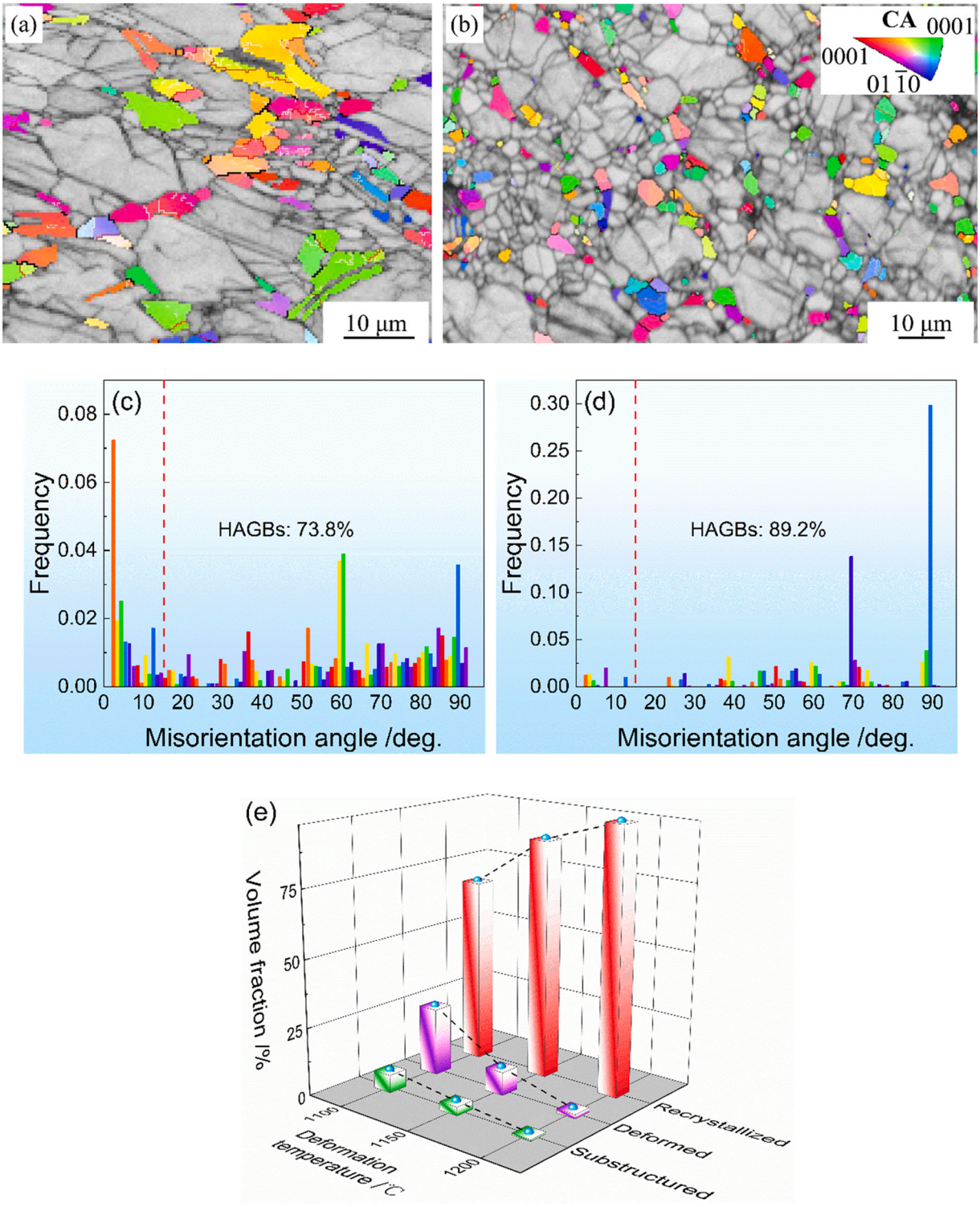

Fig. 7. (a)-(b) Inverse pole figures for α_2 phase of γ-TiAl alloy isothermally compressed at a temperature of 1200 ℃ and a strain rate of 0.01 s^{-1}: (a) 20%, (b) 50%. (γ and β_0 phases are presented by band contrast.). (c)-(d) Distribution histograms of grain boundary misorientation for γ phase of γ-TiAl alloy isothermally compressed at a strain rate of 0.001 s^{-1} up to a strain of 50%: (c) 1200 ℃, (d) 1250 ℃ [77]. (e) Effect of deformation temperature on the volume fraction for β_0 grains when γ-TiAl alloy isothermally compressed at 0.01 s^{-1}, 50% [79].

rolling temperature increases from 1200 ℃ (in (α+β+γ) phase field) to 1250 ℃ (in β phase field), the texture components of γ phase change from {031} < $\bar{5}\bar{1}$3> and {112} < 1$\bar{1}$0> to {$\bar{2}$15} < 5$\bar{5}$3> and {110} < 001] [104].

The sheet texture evolution during hot rolling of γ-TiAl alloys is influenced by many behaviors, such as deformation, recrystallization and phase transformation. Fig. 9 exhibits the influence of rolling temperature on texture components in γ, α_2 and β_0 phases during hot rolling of TNM alloy. As shown in Fig. 9, components and intensities of sheet textures in γ phase are dependent on rolling temperature, while sheet textures in α_2 and β_0 phases are less sensitive to rolling temperature. The sheet texture components for α_2 phase are {0001}

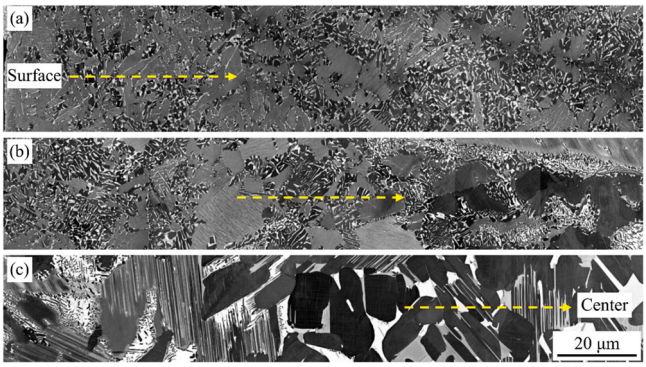

Fig. 8. SEM-BSE images of laser-remelted and heat-treated TNM alloy: (a) edge, (b) middle, (c) core (From left to right, the distance to the edge gradually increases) [100].

basal and $\{11\bar{2}0\}$ < 0001> transverse textures. And that for β_0 phase are $\{111\}$ < $\bar{1}\bar{1}2$>, $\{112\}$ < $1\bar{1}0$> brass and $\{001\}$ < 110> recrystallization textures. Apparently, texture components in α_2 and β_0 phases are more stable than in γ phase during hot rolling of TNM alloy. Similar rules can be found during hot rolling and post-heat treatment of TNM alloy. This is because rolling temperature and post-heat treatment have less impact on the phase content, dislocations density and recrystallization behavior of α_2 and β_0 phases rather than of γ phase [105,106].

Furthermore, much attention is focused on the fiber texture evolution during additive manufacturing of γ-TiAl alloys. During EBM of γ-TiAl alloy, intensities for fiber texture in γ and β_0 phases concurrently increase with the increase of electron beam energy [107]. During laser additive manufacturing of γ-TiAl alloy, the intensity for < 111 > fiber texture in γ phase increases from 16.2 mud to 32.0 mud as the laser energy increases from 1.0 kW to 2.2 kW [108]. In the meantime, the intensity for < 0001 > fiber texture in α_2 phase significantly increases from 52.1 mud to 153.4 mud.

3. Mechanical properties

Strength is one of the mechanical properties indicators for metallic materials in service. The four strengthening effects for metallic materials are solution strengthening, precipitation strengthening, grain refining strengthening and strain strengthening effects. In fact, microstructure control methods in Part 2.4 are also useful for strengthening γ-TiAl alloys. The addition of Nb atom in γ-TiAl alloys is the reflection of solution strengthening, since Nb atom substitutes Ti atom occupation in γ and α_2 phases, and Al atom occupation in β_0 phase [109,110]. Howbeit the addition of Si element is the reflection of precipitation strengthening owing to the introduced silicide. Processing route optimization can refine grain size and lamellar spacing, or can introduce twin interfaces, reflecting the grain refining strengthening. The introduction of multiple energy fields auxiliary and additive manufacturing also refine the microstructure of γ-TiAl alloys. Yet plastic pre-deformation would introduce dislocations in γ-TiAl alloys, which is a method standing for strain strengthening. In practice, γ-TiAl alloys are synergistically strengthened via various strengthening effects. This section summarized the compressive, tensile, creep and fatigue properties of γ-TiAl alloys strengthened by the above effects.

3.1. Compressive property

Compressive property is not just an indicator to evaluate the bearing capacity of γ-TiAl alloys in service, but also an indicator to predict the workability of γ-TiAl alloys during compression manufacturing. Beyond question, processing parameters are external factors influencing the compressive property of γ-TiAl alloys. Fig. 10 shows true stress-strain curves when γ-TiAl alloy with duplex structure isothermally compressed at various parameters. As seen from Fig. 10, the compressive stress of γ-TiAl alloy sharply increases to peaks and then decreases with the increase of strain. At a given strain, the compressive stress decreases with the increase of deformation temperature or decrease of strain rate. The maximum

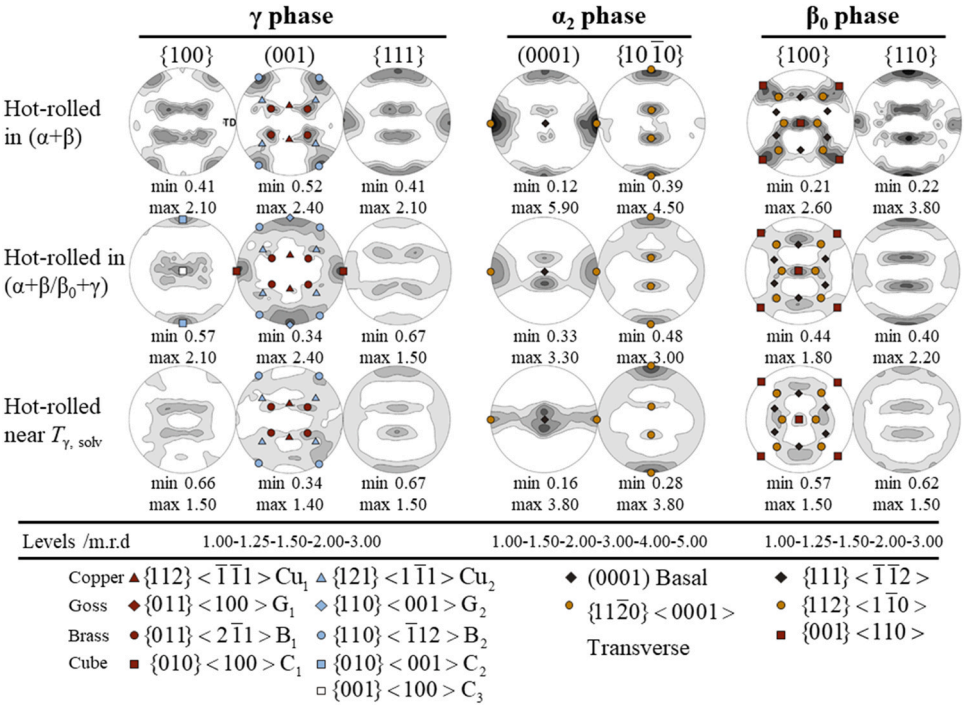

Fig. 9. Pole figures for γ, α_2 and β_0 phases of TNM alloy hot rolled at various temperatures [106].

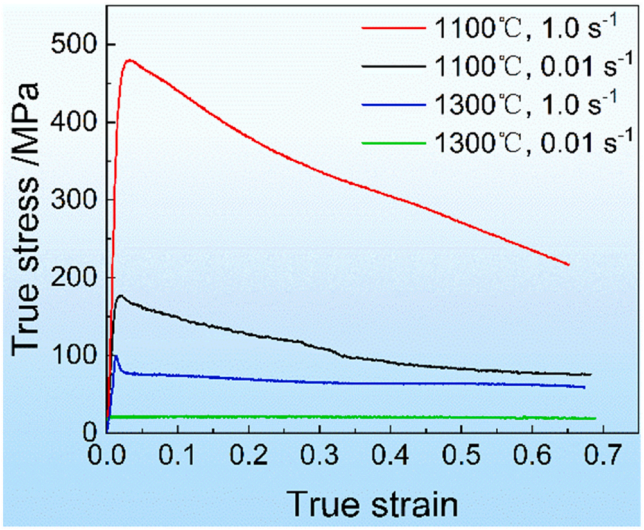

Fig. 10. True stress-strain curves during isothermal compression of duplex γ-TiAl alloy [111].

compressive stress is 479.9 MPa. Admittedly, the change of compressive stress is tightly linked to the change of dislocation density caused by recrystallization and phase transformation in γ-TiAl alloy [111,112].

As mentioned earlier, adequate alloying elements like Nb element would induce solution strengthening, and thus influence the compressive property of γ-TiAl alloys. Wang et al. [64] reported that adding Mn element significantly improves the yield stress, compressive stress and relative compressibility of γ-TiAl alloy at ambient temperature. Especially, the compressive stress of γ-TiAl alloy improves by about 42.14% with the Mn element content of 1 at.%. Adding 1 at.% Sn element also increases the compressive stress of γ-TiAl alloy up to 3029 MPa with the extent of 6.88% [113]. Except for elements inherence and experimental measurement difference, the difference in solution strengthening effect of Mn and Sn elements can be ascribed to the difference in distributions. Mn element is concentrated in soft-elastic β_0 phase [68]. Yet Sn is enriched in hard α_2 phase of γ-TiAl alloy [113]. Undoubtedly, alloying elements have a more significant solution strengthening effect on soft-elastic phase than on hard one.

C element is mainly distributed in γ and α_2 phases, showing a complicated strengthening effect in γ-TiAl alloy. Fang et al. [73] studied the influence of C content on the strengthening effect of γ-TiAl alloy compressed at room temperature. When the adding content is lower than 1.0 at.%, C atoms are mainly distributed in α_2 phase as interstitial atoms, and the strengthening effect is solution strengthening. When further increasing the C content, C atoms are enriched in α_2 phase as H-Ti_2AlC, and the strengthening effect switches to precipitation strengthening effect. Additionally, under the precipitation strengthening effect, the compressive stress of γ-TiAl alloys reaches the peak (2324.3 MPa) with the C content of 1.5 at.%, and the relative compressibility subsequently achieves the peak (28.1%) when C content increases to 2.5 at.%.

The introduction of minor phases or precipitation particles also influences the compressive property of γ-TiAl alloys. Introducing τ_2 phase can significantly increase the room-temperature compressive stress and relative compressibility of γ-TiAl alloy [34]. Introducing TiB_2 particles increases the delamination tendency of α_2/γ lamellar colonies, resulting in the deterioration of compressive property when γ-TiAl alloys are compressed at high-temperature [43].

Furthermore, fabrication parameters would influence the compressive property of γ-TiAl alloys fabricated via additive manufacturing. With the decrease of electron beam intensity from 8.5 mA to 4.5 mA, the compressive stress of γ-TiAl alloys increases from 2456.8 MPa to 2931.0 MPa, and the relative compressibility increases from 27.50% to 34.81% during room-temperature compression [114]. There is no doubt that the compressive property improvement of EBM-fabricated γ-TiAl alloys is related to the increase in the size and volume fraction of α_2/γ lamellar colonies.

3.2. Tensile property

The strengthening effect of elements on tensile property of γ-TiAl alloys is attributed to solution and/or precipitation strengthening effect. Adding Nb element increases the elongation to failure at room temperature, because Nb element decreases the intrinsic stacking fault energy and alternates deformation modes of γ phase [115,116]. The addition of Ni element increases ultimate strength and elongation to failure of γ-TiAl alloy under tensile deformation at room and high temperature, resulting from the volume fraction increase in γ phase and τ_3 phase (Al_3NiTi_2) nanoparticles [117]. As C content increases, both the ultimate strength and elongation to failure of γ-TiAl alloys firstly increase and then decrease, which are relevant to the carbides evolutions during room and high temperature tensile tests [73,118].

Usually, particles only play the precipitation strengthening effect on γ-TiAl alloys. Adding 2 wt% WC nanoparticles can noticeably increase the ultimate strength of γ-TiAl alloy by the extent of 51.07%, and the elongation to failure by 80.95% at room temperature [119]. And the maximum ultimate strength and elongation to failure are 826.77 MPa and 3.87%, respectively. Moreover, adding Y_2O_3 or TiB particles can effectively promote the tensile property of γ-TiAl alloys tested at 800 ℃ [120,121]. Specially, the improvement of B_4C particles on high temperature tensile property of γ-TiAl alloys is not only connected to the precipitation strengthening of TiB particles, but also linked to the solution strengthening of C element [122].

Optimizing preparation routes also enhances the tensile property of γ-TiAl alloys [123]. Fig. 11 displays the tensile property of 4822 alloy fabricated via suction casting (SC) and traditional casting (TC). As seen from Fig. 11, the ultimate strength of SC 4822 alloy is much higher than that of TC 4822 alloy, and so does the elongation to failure. Additionally, the ultimate strength decreases and the elongation to failure increases with the increasing of testing temperature. The room-temperature tensile property of γ-TiAl alloy fabricated via electromagnetic cold crucible directional solidification (ECCDS) is higher than that of TC γ-TiAl alloy [124]. For 4822 alloys fabricated via ECCDS, the ultimate strength at room temperature dramatically increases from 161.8 MPa to 590.6 MPa, and the

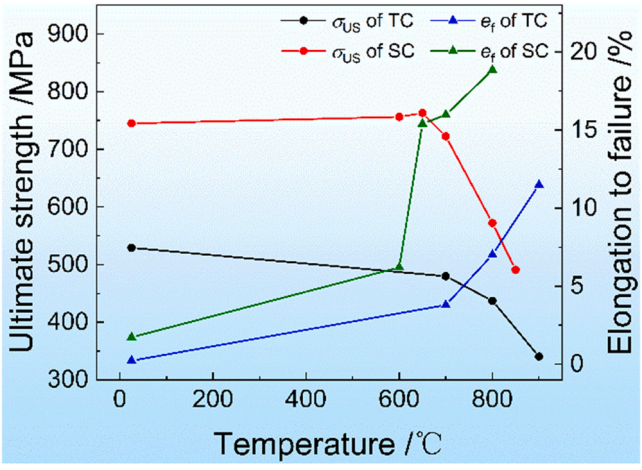

Fig. 11. Tensile property of 4822 alloy tested at various temperatures [126].

elongation to failure concurrently increases from 1.01% to 2.05%, as the pulling rate increases from 5 μm·s^{-1} to 15 μm·s^{-1} [125].

Heat treatments are widely used to promote the tensile property of γ-TiAl alloys, too. After proper heat treatment, the tensile deformation mode of γ-TiAl alloys at room temperature switches from dislocation slip to twinning, and thus improving the tensile property of γ-TiAl alloys [76]. Cyclic heat treatments also enhance the tensile property of γ-TiAl alloy [127,128]. Through cyclic heat treatment and series aging treatments, Yim et al. [74] fabricated γ-TiAl alloy with the ultimate strength at room temperature up to 697 MPa and γ-TiAl alloy with the maximum elongation to failure at room temperature of 2.3%. However, applied short aging treatments in the α single-phase field decreases the tensile property of γ-TiAl alloys, and the minimum elongation to failure is only 0.67%. Interestingly, long-time annealing at 800 ℃ does not deteriorate the room-temperature and high-temperature tensile properties of γ-TiAl alloy [129].

Like hot extrusion [130] and forging [131], pre-deformation also changes the tensile property of γ-TiAl alloys. Compared with γ-TiAl alloy without hot extrusion, γ-TiAl alloy extruded at 1300 ℃ to the extrusion ratio of 9 shows a higher tensile property at room and high temperature [132]. Among them, the ultimate strength at room temperature increases from 437.9 MPa to 865.6 MPa after hot extrusion.

Some efforts also have been paid to improve the tensile property of γ-TiAl alloys fabricated by additive manufacturing. Al content has a large impact on room-temperature tensile property of binary γ-TiAl alloys prepared by twin-wire plasma arc additive manufacturing, and the maximum ultimate strength and elongation to failure achieved with the Al content of 48 at.% [12]. With the increasing of electron beam intensity, the ultimate strength firstly increases and then decreases, while the elongation to failure gradually increases to 0.98% during room-temperature tensile deformation of EBM-fabricated γ-TiAl alloy [107]. With regard to γ-TiAl alloys fabricated by selected laser melting, ultimate strength at room temperature increases to 543.4 MPa and the elongation to failure increases to 3.7% after γ-TiAl alloys annealed at 1260 ℃ for 30 min [133].

3.3. Creep property

Creep property is the mechanical property indicator for γ-TiAl alloys to maintain component dimensional stability in service [134]. As seen from Fig. 12a, the creep rate of γ-TiAl alloys sharply decreases and then increases with the proceeding of creep (the increasing of creep strain). With the increasing of creep stress from 120 MPa to 300 MPa, the creep rate of γ-TiAl alloys increases but the rupture life decreases from 161.5 h to 1.6 h (Fig. 12a-b).

Adding elements remarkably improves the creep property of γ-TiAl alloys. Adding Hf and Zr elements decreases the creep rate of γ-TiAl alloys [71]. In addition, γ-TiAl alloy containing both Hf and Zr elements presents the minimum creep rate when crept at the temperature of 700 ℃ and the stresses of 250 and 350 MPa. Adding W element also promotes creep resistance of γ-TiAl alloys, because W atoms can effectively pin dislocations movement in γ phase [135].

Introducing particles also increases the creep property of γ-TiAl alloys [120]. After adding 0.05 at.% Y_2O_3 particles, the rupture life of 4822 alloy increases from 45.1 h to 150.0 h, and the minimum creep strain decreases from 26.7 to 18.1 when 4822 alloy crept at 800 ℃/300 MPa [137]. Carbide particles, like H-Ti_2AlC and P-Ti_3AlC, are also widely added in γ-TiAl alloys to promote the creep resistance of γ-TiAl alloys. Unlike Y_2O_3 particles, the strengthening effect of carbide particles on the creep property of γ-TiAl alloys varies with the content and morphology of carbide particles [46].

Heat treatment also can enhance the creep property of γ-TiAl alloys. Compared with γ-TiAl alloy without heat treatment, the rupture life for γ-TiAl alloy after heat treated at 1380 ℃ for 1–2 h is much higher when creep tests are conducted at 800 ℃/220 MPa, resulting from the increase in volume fraction of α_2/γ lamellar colonies [138]. After aging treatment, the creep property of γ-TiAl alloy is significantly promoted by β_0 phase particles formed on α_2/γ lamellar interfaces [139].

3.4. Fatigue property

In the service process, metallic components often bear cyclic loads. In some cases, metallic components might suddenly fracture without warning, and the stress level at the time is lower than the permissible stress, indicating the fracture is induced by fatigue. Generally, the fatigue life decreases with the increasing of cyclic stress level. The cycles for low-cycle fatigue (LCF) are lower than 10^5 cycles, and cycles for high-cycle fatigue (HCF) are 10^5-10^7 cycles.

During aero engines running, LPT blades are inevitably subjected to centrifugal loads. The further away from the LPT disc, the greater centrifugal loads that LPT blades bear. In other words, HCF happens at the head of LPT blades, and LCF might occur at the root of LPT blades. Thereby, elucidating the fatigue property of γ-TiAl alloys is an important premise for ensuring safety in service of γ-TiAl alloys components. Heretofore, intensive efforts have been paid to study the HCF and LCF fatigue properties of γ-TiAl alloys, as described in the following.

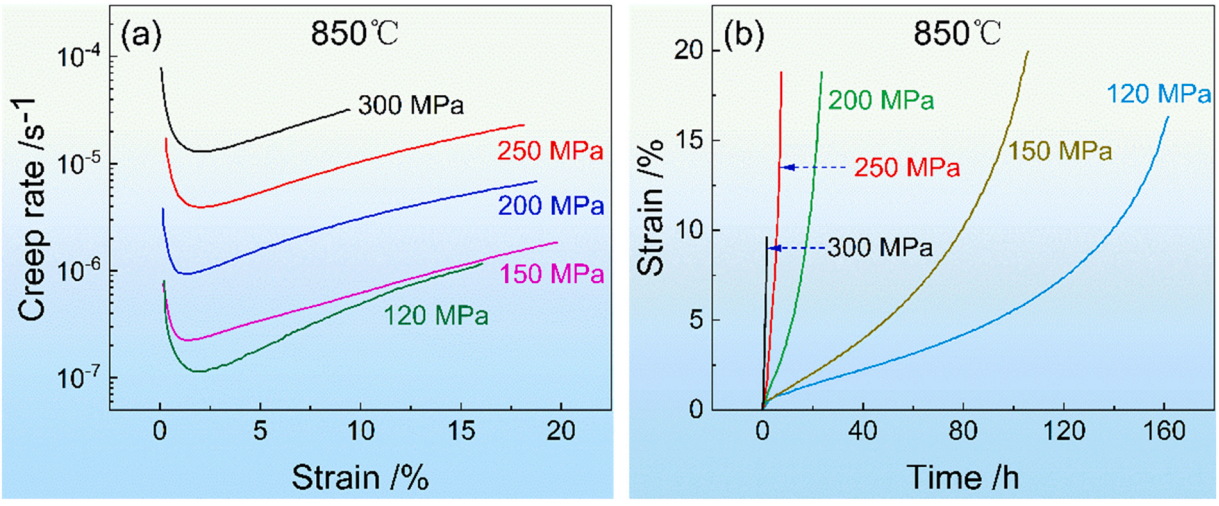

Fig. 12. (a) Creep rate-strain and (b) creep strain-time curves of Ti-44.6Al-7.9Nb-3.6C-0.7Mo-0.1B at 850 ℃ [136].

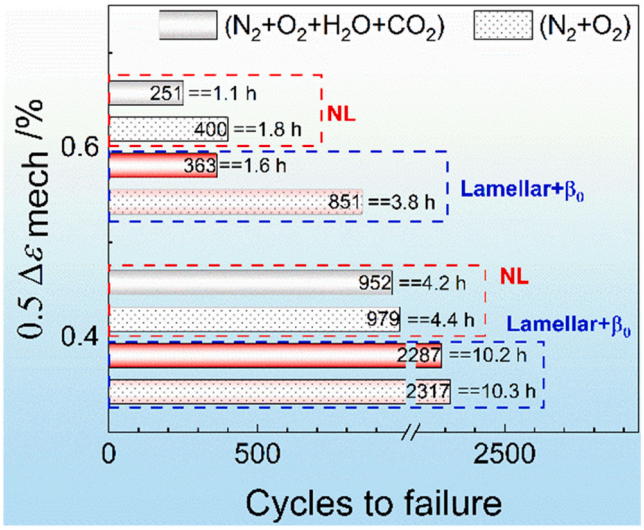

Fig. 13. Cyclic strain response curves of γ-TiAl alloys tested in various atmospheres [146].

3.4.1. Low cycle fatigue property

Ding et al. [140] studied the LCF behavior of γ-TiAl alloys with fully lamellar structure. With the increasing of LCF cycles, the cyclic stress amplitude gradually decreases, while the cyclic strain amplitude gradually increases, showing a cyclic softening phenomenon. This phenomenon is mainly caused by static recrystallization in γ-TiAl alloys with fully lamellar structure. As for γ-TiAl alloys with duplex structure, the cyclic softening phenomenon is induced by phase transformation and static recrystallization of γ phase [141]. In the LCF process, the change of internal stress state induces the formation of hard ω_0 phase and the initiation of cracks, thereupon results in premature failure of γ-TiAl alloys [142]. As for γ-TiAl alloys fabricated by additive manufacturing, the LCF property is related to the angle (θ) between fabrication direction and fatigue loading direction. In comparison with EBM-fabricated γ-TiAl alloy with the θ of 0°, the alloy with the θ of 40° presents longer fatigue life at room temperature [143]. However, the fatigue life at 750 ℃ seems independent of the angle between electron beam scanning direction and fatigue loading direction.

Fatigue property of γ-TiAl alloys is not only affected by microstructure characteristics, but also influenced by cyclic strain amplitude and experimental atmosphere. Fig. 13 shows the influence of cyclic strain amplitude, microstructure and experimental atmosphere on fatigue life of γ-TiAl alloys at 850 ℃. As seen from Fig. 13, the fatigue life decreases with the increase of cyclic strain amplitude. The fatigue life of γ-TiAl alloy with nearly lamellar structure is lower than that with (lamellar+β_0) structure, which is resulted from the β_0 phase in a necklace distribution. But the fatigue life of γ-TiAl alloy tested in (N_2+O_2) atmosphere is much higher than that tested in (N_2+O_2 +H_2O+CO_2) atmosphere, due to the absence of dense TiN layer. In the above cases, the fatigue property of γ-TiAl alloys is complicated and tightly linked to their oxidation behaviors.

Practically, creep and fatigue might concurrently occur when metallic components are in service. Some researchers [144,145] focused on the mechanical property of γ-TiAl alloys under the interaction between LCF and creep, which are not reiterated here. Considering the high strength and poor plasticity, the LCF property is the crucial indicator for γ-TiAl alloys to be utilized as large-size LPT blades. Hence relevant studies on the LCF property of γ-TiAl alloys should be highlighted in later research.

3.4.2. High cycle fatigue property

Throughout the HCF testing, the loading stress level is lower than the yield stress of metallic components, meaning that only elastic deformation occurs during HCF testing. The HCF cycle decreases with the increasing of loading stress level. Ideally, some metallic components can infinitely serve without fracture under a certain stress level, and the critical stress level is termed as “endurance limit”. Loading type and specimen integrity are external factors influencing the HCF property of γ-TiAl alloys. According to Ref. [147], the HCF fatigue life of γ-TiAl alloys tested under cyclic tensile loads is higher than that under cyclic torsional loads. The sound γ-TiAl alloy specimens can bear much higher loading stress amplitude than the notched ones, as presented in Fig. 14a, for that stress is concentrated at the notch. Besides, for γ-TiAl alloys, the sensitivity of HCF property to notch increases with the increase of grain size [148].

γ-TiAl alloys fabricated via ECCDS technology possess higher fatigue property than γ-TiAl alloys fabricated via traditional casting (Fig. 14b). According to digital image correlation (DIC) technology, it is revealed that the fatigue strain distribution is quite heterogonous during room-temperature HCF testing of γ-TiAl alloy with fully lamellar structure [149]. Xu et al. [150] even claimed that the HCF damage is accumulated in γ lamellae of γ-TiAl alloys. However, Chen et al. [151] found that the fatigue strain distribution in PST-TiAl single crystal is relatively uniform. This is because < *c*+*a* > dislocations in α_2 lamellae can effectively accommodate the fatigue strain during HCF testing at high temperature.

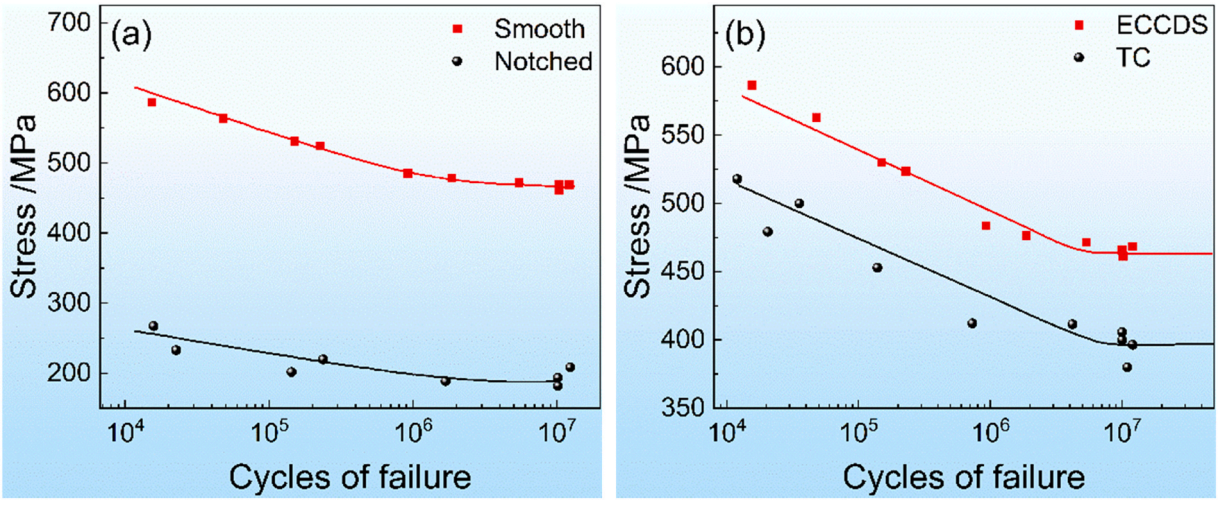

Fig. 14. *S-N* curves of (a) smooth and notched γ-TiAl alloys fabricated via ECCDS [150], (b) γ-TiAl alloys fabricated via TC and ECCDS [152].

The HCF property of γ-TiAl alloys is also related to the surface quality of specimens. Surface finish technologies, like electro polishing, shot peening and turning polishing, can decrease the surface roundness of γ-TiAl alloys specimens. After surface finish, both loading stress level and sensitivity of HCF property to notch increase when γ-TiAl alloys were HCF tested at room temperature [148,153]. Apart from surface roundness, thermal exposure in air might deteriorates the fatigue life of γ-TiAl alloys HCF tested at high temperatures, for the reason that large amounts of β_0 phase are formed in the surface layer [154]. However, Huang et al. [148] claimed that thermal exposure in air plays a complex influence on the HCF property of γ-TiAl alloys at room temperature. If thermal exposure in air only induces microstructure evolution, then it would prolong the HCF life of γ-TiAl alloys. If thermal exposure in air facilitates the surface oxidation, then it would prolong the HCF life for unpolished γ-TiAl alloys, and shorten the HCF life for γ-TiAl alloys after surface polishing.

4. Tribological property

During the machine running period, relative movement is inevitable between components and supporting mediums or other contacting components, which gives rise to friction. So indicating the tribological property of metallic components is also one of the prerequisites to ensure safety in service of components. Unlike mechanical properties in Part 3, tribological property is the mechanical property of metallic materials under contact stress.

Wear loss and friction coefficient are often used to evaluate the tribological property of metallic materials. As the wear cycle increases, the wear rate firstly increases and then gradually decreases during the fretting wear of γ-TiAl alloy, which is ascribed to the formation of tribo-layers with high oxygen content [155]. With the increasing of sliding speed or decreasing of contacting stress, the friction coefficient of γ-TiAl alloy gradually increases [156]. Besides, with increasing sliding speed, the wear loss of γ-TiAl alloy decreases, because the wear mechanism switches from abrasive to oxidation wear [157]. Moreover, with increasing testing temperature, the wear loss firstly increases and then decreases, while the friction coefficient gradually decreases during high-temperature wear of γ-TiAl alloy [158].

Fig. 15 shows the effect of Nb content on wear loss and friction coefficient of γ-TiAl alloys. As seen from Fig. 15, the wear loss and friction coefficient of γ-TiAl alloys firstly decrease and then increase with the increasing of Nb content from 3 at.% to 6 at.%. Interestingly, further adding Nb content to 7 at.% would significantly decreases the wear loss and friction coefficient of γ-TiAl alloys. This might be attributed to the solution strengthening effect induced by Nb element, and the transformation of microstructure to nearly lamellar structure [159]. Hua et al. [160] found that the wear loss of γ-TiAl alloy with lamellar structure is quite lower than that with duplex structure, while the friction coefficient is close to that with duplex structure. As for PST-TiAl single crystal, the tribology property is tightly linked to the orientation. As the included angle between sliding direction and lamellar interface increases, the wear loss of PST-TiAl single crystal decreases while the friction coefficient gradually increases [157].

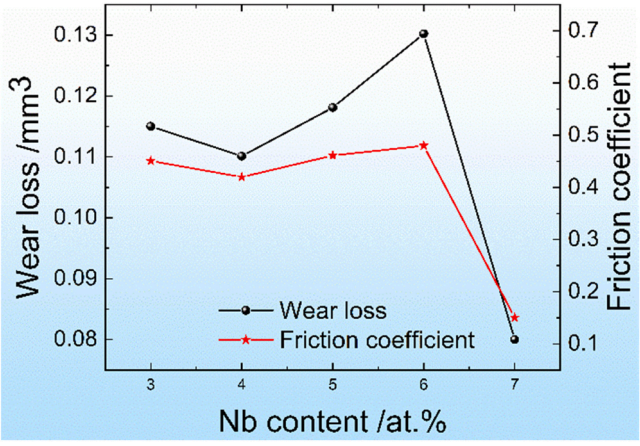

Fig. 15. Effect of Nb content on wear loss and friction coefficient of γ-TiAl alloys [159].

Adding particles also affect the tribological property of γ-TiAl alloys. Cheng et al. [156] claimed that adding TiB_2 particles has no impact on the friction coefficient, but increases the wear resistance of γ-TiAl alloy. This is because adding TiB_2 particles increases the Vickers hardness of γ-TiAl alloy. Likewise, adding H-Ti_2AlC particles slightly increases the friction coefficient and wear resistance of γ-TiAl alloy, due to the precipitation strengthening effect of H-Ti_2AlC particles with network distributions [161]. Moreover, coating treatment would enhance the tribological property of γ-TiAl alloys. After coating $TiAl_3$ films with the thickness of 30 μm, both the wear loss and friction coefficient of γ-TiAl alloys are effectively reduced during friction tests at room and high temperature [158].

Furthermore, testing atmosphere and contacting materials would influence the tribology property of γ-TiAl alloys. As seen from Fig. 16, the wear loss of γ-TiAl alloys tested in O_2 atmosphere is much higher than that tested in oxygen-free atmospheres, like (H_2+N_2) and Ar atmosphere [162]. Additionally, the wear loss of γ-TiAl alloy with high Nb content ((Ti-45Al-5 Nb-0.4 W)+ 2 Nb) is much higher than that with low Nb content (Ti-47Al-2 Nb-2Cr-0.2 W). Similarly, Qiu et al. [163] found that adding Nb element decreases the wear loss of γ-TiAl alloys tested in oxygen-containing atmosphere. Moreover, increasing the hardness of contacting materials would increase the wear loss and friction coefficient of γ-TiAl alloys [164].

5. Fracture mechanism

Fatigue, wear and fracture are the main failure mechanisms during workpiece running, among which fracture is most harmful. Fracture is a phenomenon that the material no longer maintains its integrity due to stress acting on it, which is tightly linked to

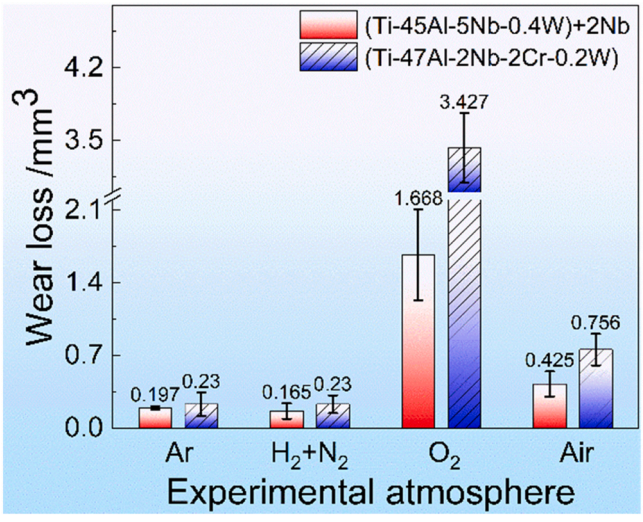

Fig. 16. Influence of experimental atmosphere on wear loss of γ-TiAl alloys when dry sliding wear tests were performed at room temperature [162].

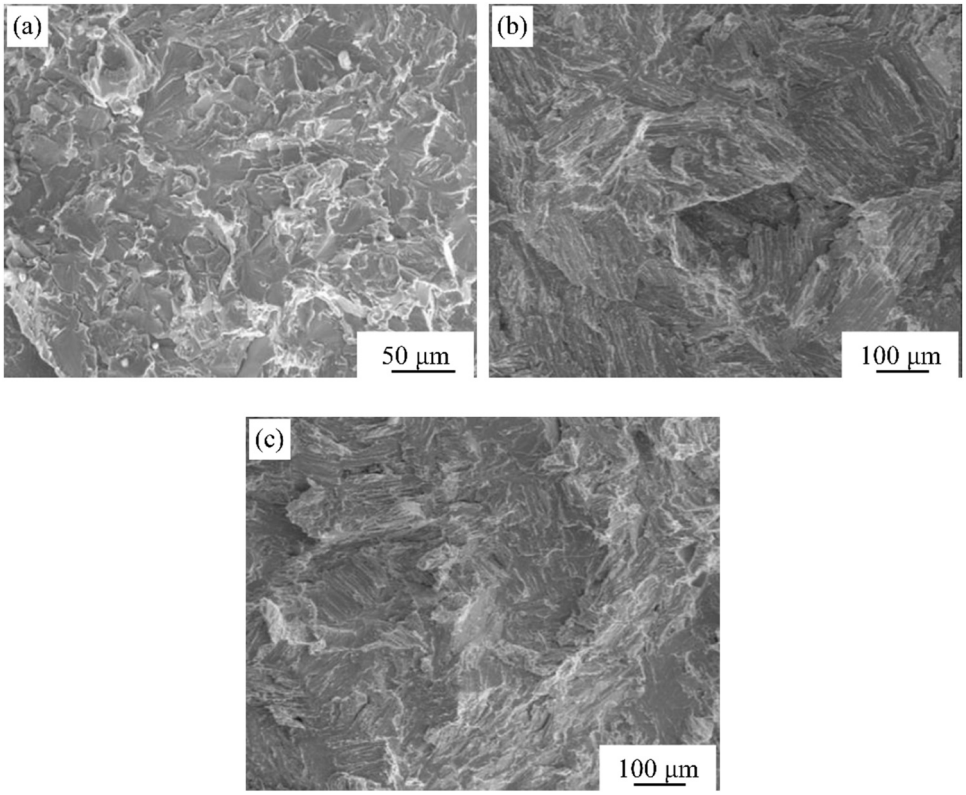

Fig. 17. Fracture surfaces of γ-TiAl alloys after 3-points bending at room temperature: (a) nearly γ structure, (b) nearly lamellar structure and (c) fully lamellar structure [168].

mechanical properties (fracture toughness) of the material. The fracture mechanisms are divided into ductile and brittle fractures, depending on whether the plastic deformation occurs before the material fracture. On the basis of crack growth routes, the fracture mechanisms are divided into trans-granular fracture and inter-granular fracture, both of which belong to the brittle fracture. This section is only a brief overview of recent research.

Raina [165] studied fracture behaviors of γ-TiAl alloys during compact tension and 3-points bending tests at room temperature. During compact tension tests of γ-TiAl alloys, the force at pin supports firstly increases to peak value and then decreases with the increasing of crack mouth opening displacement. And during 3-points bending of γ-TiAl alloys, the fracture energy density significantly decreases as the height of specimens increases. The fracture toughness of PST-TiAl single crystal keeps the classical Hall-Petch relationship to lamellar spacing, while it shows an inverse Hall-Petch relationship to lamellar spacing when the lamellar spacing is lower than 1.64 nm [166]. With the increasing of intersection angle between lamellar interface and initial crack plane, the fracture toughness of PST-TiAl single crystal gradually increases, and the fracture mechanism switches from inter-lamellar to trans-lamellar fracture [167]. The fracture behaviors of polycrystalline γ-TiAl alloys are tightly related to microstructure characteristics. As the volume fraction of α_2/γ lamellar colonies increases, the fracture toughness of γ-TiAl alloys increases [168]. As seen from Fig. 17, the fracture modes for γ-TiAl alloy with nearly γ structure are inter-granular and trans-granular fracture, while that for γ-TiAl alloy with nearly and fully lamellar structure are inter-lamellar and trans-lamellar fracture. The increasing of fracture toughness is ascribed to shear band bridging, cracks deflection and branching [169]. Additionally, β_0 phase distributed along α_2/γ lamellar colonies boundaries would induce cracks branching and increase the fracture toughness [168]. However, if hard ω_0 phase precipitated from β_0 phase, the fracture toughness would worsen and inter-lamellar fracture would occur in γ-TiAl alloys [170]. Appel. et al. [171] found that the residual macrostrain and reversion of strain path can inhibit cleavage fracture of γ-TiAl alloys. Compared to γ-TiAl alloys fabricated by selective electron beam melting, γ-TiAl alloys fabricated by electron beam smelting shows higher fracture toughness, which is resulting from cracks deflection and branching [95]. Briefly, the room-temperature fracture mechanism of γ-TiAl alloys is brittle fracture.

As the deformation temperature increases, the tensile ductility of γ-TiAl alloys is gradually improved, and the tensile fracture mechanism switches from brittle to ductile fracture. The brittle-ductile transition temperature (BDTT) of γ-TiAl alloys is 600–920 ℃ [126,172]. When the tensile temperature is lower than the BDTT, the fracture mechanism of γ-TiAl alloys is inter-lamellar fracture, as presented in Fig. 18a. As the temperature increases to 800 ℃, intensive tearing ridges can be found on the fracture surface (Fig. 18b), indicating that the fracture mode of γ-TiAl alloys is still brittle fracture. When the tensile temperature is higher than the BDTT, a large number of dimples can be found on the fracture surface (Fig. 18c), suggesting that the fracture mode of γ-TiAl alloys switches into ductile fracture.

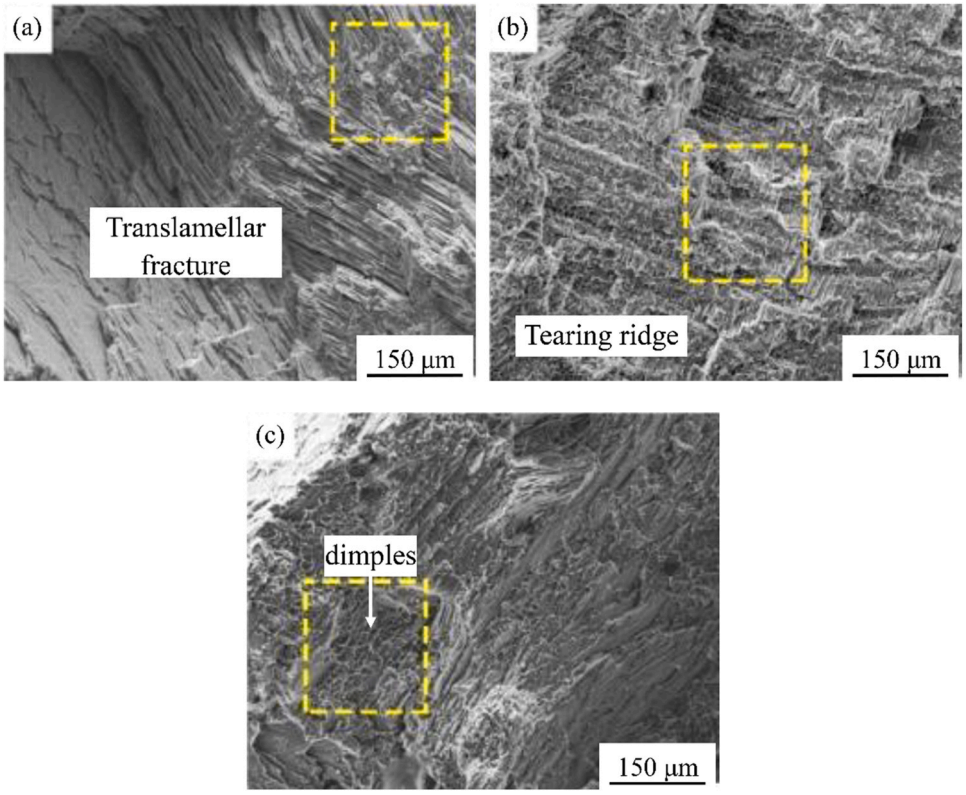

Fig. 18. Fracture surfaces of γ-TiAl alloys after high-temperature tensile tests: (a) 700 ℃, (b) 800 ℃, (c) 900 ℃ (The BDTT is 750–800 ℃) [69].

6. Conclusions and prospects

Based on the relationship between microstructure and performance, the authors reviewed phase constituents and precipitates of γ-TiAl alloys, and summarized various microstructure control routes, like chemical composition design, processing route optimization and other energy fields auxiliary. Also, the microstructure of γ-TiAl alloys fabricated via additive manufacturing was reviewed, and so did the texture of γ-TiAl alloys. Moreover, the authors summarized mechanical properties, like compressive, tensile, creep and fatigue properties of γ-TiAl alloys. Finally, the tribological property and fracture mechanisms of γ-TiAl alloys are also reviewed. Albeit intensive efforts have been paid on γ-TiAl alloys, following research are still needed to solve in the future.

(1) Introducing new technologies like machine learning, to assist in screening chemical compositions of γ-TiAl alloys.
(2) Identifying formation conditions of minor phases via computational simulation technologies, elucidating the effect of minor phases and microstructure characteristics on mechanical properties and tribology property of γ-TiAl alloys, and establishing the mapping relationship between process, microstructure and performance.
(3) Establishing microstructure evaluation methods of γ-TiAl alloys, and developing the corresponding software with high efficiency and accuracy.
(4) Designing special microstructure characteristics, like gradient structure, to meet the service scene and performance requirements of γ-TiAl alloys.
(5) Systemically clarifying microstructure evolutions and mechanical properties changes during additive manufacturing of γ-TiAl alloys, and also that in the fabrication process assisted by multi-energy fields.

Data Availability

No data was used for the research described in the article.

Declaration of Competing Interest

The authors declare that they have no known competing financial interests or personal relationships that could have appeared to influence the work reported in this paper.

Acknowledgments

The authors acknowledge financial supports from the National Key Research and Development Program of China (Grant No. 2017YFA0204403), National Natural Science Foundation of China (Grant No. 51971112 and 51225102), the Fundamental Research Funds for the Central Universities (Grant No. 30919011405) and the Open Fund for Large Instruments and Equipments of Nanjing University of Science and Technology.

References

[1] Y. Gao, S. Chien, Review on space robotics: Toward top-level science through space exploration, Sci. Robot. 2 (2017) eaan5074.
[2] D.D. Gu, X.Y. Shi, R. Poprawe, D.L. Bourell, R. Setchi, J.H. Zhu, Material-structure-performance integrated laser-metal additive manufacturing, Science 372 (2021) eabg1487.
[3] C. Leyens, M. Peters, Titanium and titanium alloys: fundamentals and applications, Wiley-VCH GmbH & Co. KGaA, Weinheim, Germany, 2003.
[4] P.D. He, R.F. Webster, V. Yakubov, H. Kong, Q. Yang, S.K. Huang, M. Ferry, J.J. Kruzic, X.P. Li, Fatigue and dynamic aging behavior of a high strength Al-5024 alloy fabricated by laser powder bed fusion additive manufacturing, Acta Mater. 220 (2021) 117312.
[5] X. Wen, M.P. Wan, C.W. Huang, M. Lei, Strength and fracture toughness of TC21 alloy with multi-level lamellar microstructure, Mater. Sci. Eng. A 740- 741 (2019) 121–129.

[6] X.W. Ye, M.P. Wan, C.W. Huang, M. Lei, S.C. Jian, Y. Zhang, D. Xu, F. Huang, Effect of aging temperature on mechanical properties of TC21 alloy with multi-level lamellar microstructure, Mater. Sci. Eng. A 840 (2022) 142825.
[7] R.R. Boyer, R.D. Briggs, The use of β titanium alloys in the aerospace industry, J. Mater. Eng. Perform. 14 (6) (2005) 681–685.
[8] G. Chen, Y.B. Peng, G. Zheng, Z.X. Qi, M.Z. Wang, H.C. Yu, C.L. Dong, C.T. Liu, Polysynthetic twinned TiAl single crystals for high-temperature applications, Nat. Mater. 15 (8) (2016) 876–881.
[9] Z.N. Zhao, L. Li, W.Z. Yang, Y. Zeng, Y.D. Lian, Z.F. Yue, A comprehensive study of the anisotropic tensile properties of laser additive manufactured Ni-based superalloy after heat treatment, Int. J. Plast. 148 (2022) 103147.
[10] H. Clemens, S. Mayer, Design, processing, microstructure, properties, and applications of advanced intermetallic TiAl alloys, Adv. Eng. Mater. 15 (2013) 191–215.
[11] S. Mayer, P. Erdely, F.D. Fischer, D. Holec, M. Kastenhuber, T. Klein, H. Clemens, Intermetallic β-solidifying γ-TiAl based alloys − from fundamental research to application, Adv. Eng. Mater. 19 (4) (2017) 1600735.
[12] L. Wang, C. Shen, Y.L. Zhang, F. Li, Y. Huang, Y.H. Ding, J.W. Xin, W.L. Zhou, X.M. Hua, Effect of Al content on the microstructure and mechanical properties of γ-TiAl alloy fabricated by twin-wire plasma arc additive manufacturing system, Mater. Sci. Eng. A 826 (2021) 142008.
[13] H.Z. Fang, R.R. Chen, X.Y. Chen, Y. Yang, Y.Q. Su, H.S. Ding, J.J. Guo, Effect of Ta element on microstructure formation and mechanical properties of high-Nb TiAl alloys, Intermetallics 104 (2019) 43–51.
[14] X.S. Xu, H.S. Ding, H.T. Huang, H. Liang, S. Kawk, R.R. Chen, J.J. Guo, H.Z. Fu, Role of growth rate on microstructure evolution, element distribution and nanohardness of phases in directionally solidified multiphase high-Nb TiAl, Alloy, J. Mater. Res. Technol. 14 (2021) 2884–2896.
[15] R.R. Xu, M.Q. Li, gamma→beta phase transformation in Ti-42.9Al-4.6Nb-2Cr, Intermetallics 133 (2021) 107169.
[16] Y.Y. Chen, H.Y. Yue, X.P. Wang, S.L. Xiao, F.T. Kong, X.K. Cheng, H. Peng, Selective electron beam melting of TiAl alloy: microstructure evolution, phase transformation and microhardness, Mater. Charact. 142 (2018) 584–592.
[17] L. Li, W. Zhao, Z.X. Feng, J. Sun, X.Q. Li, Microstructure and shear strength of γ-TiAl/GH536 joints brazed with Ti-Zr-Cu-Ni-Fe-Co-Mo filler alloy, T. Nonferrous Metal. Soc. 30 (8) (2020) 2143–2155.
[18] P.V. Panin, A.S. Kochetkov, A.V. Zavodov, E.A. Lukina, Effect of Gd addition on phase composition, structure, and properties of beta-solidifying TiAl-based alloy with Zr and Cr content variability, Intermetallics 121 (2020) 106781.
[19] X.Y. Wang, J.R. Yang, K.R. Zhang, R. Hu, L. Song, H.Z. Fu, Atomic-scale observations of B2→ω-related phases transition in high-Nb containing TiAl alloy, Mater. Charact. 130 (2017) 135–138.
[20] T. Ye, L. Song, S.B. Gao, Y.F. Liang, Y.L. Wang, J.P. Lin, Precipitation behavior of the ω_0 phase in an annealed high Nb-TiAl alloy, J. Alloy. Compd. 701 (2017) 882–891.
[21] M.W. Rackel, A. Stark, H. Gabrisch, N. Schell, A. Schreyer, F. Pyczak, Orthorhombic phase formation in a Nb-rich γ-TiAl based alloy – an in situ synchrotron radiation investigation, Acta Mater. 121 (2016) 343–351.
[22] D.X. Li, G.Y. Zhang, G. Lu, Y.J. Liu, J.J. Wang, C.M. Liu, Precipitation of Ti_2Al phases at lamellar interfaces in a high-Nb-containing TiAl alloy during thermal exposure, J. Mater. Sci. Technol. 126 (2022) 132–140.
[23] M.G. Li, S.L. Xiao, Y.Y. Chen, L.J. Xu, J. Tian, The effect of boron addition on the deformation behavior and microstructure of β-solidify TiAl alloys, Mater. Charact. 145 (2018) 312–322.
[24] Z.W. Huang, Ordered ω phases in a 4Zr-4Nb-containing TiAl-based alloy, Acta Mater. 56 (8) (2008) 1689–1700.
[25] L. Song, L.Q. Zhang, X.J. Xu, J. Sun, J.P. Lin, Omega phase in as-cast high-Nb-containing TiAl alloy, Scr. Mater. 68 (12) (2013) 929–932.
[26] L. Song, X.G. Hu, T.B. Zhang, J.S. Li, Precipitation behaviors in a quenched high Nb-containing TiAl alloy during annealing, Intermetallics 89 (2017) 79–85.
[27] L. Song, F. Appel, L. Wang, M. Oehring, X.G. Hu, A. Stark, J.Y. He, U. Lorenz, T.B. Zhang, J.P. Lin, F. Pyczak, New insights into high-temperature deformation and phase transformation mechanisms of lamellar structures in high Nb-containing TiAl alloys, Acta Mater. 186 (2020) 575–586.
[28] L. Song, F. Appel, A. Stark, U. Lorenz, J.Y. He, Z.B. He, J.P. Lin, T.B. Zhang, F. Pyczak, On the reversibility of the α_2/ω_0 phase transformation in a high Nb containing TiAl alloy during high temperature deformation, J. Mater. Sci. Technol. 93 (2021) 96–102.
[29] C.R. Dai, Z.B. Yang, J. Sun, S. Lu, L. Vitos, Composition and temperature dependence of α_2 phase decomposition in high Nb-containing lamellar γ-TiAl alloys: Experiments and first-principles calculations, Acta Mater. 221 (2021) 117419.
[30] G.D. Ren, J. Sun, High-resolution electron microscopy characterization of modulated structure in high Nb-containing lamellar γ-TiAl alloy, Acta Mater. 144 (2018) 516–523.
[31] M. Musi, P. Erdely, B. Rashkova, H. Clemens, A. Stark, P. Staron, N. Schell, S. Mayer, Evidence of an orthorhombic transition phase in a Ti-44Al-3Mo (at.%) alloy using in situ synchrotron diffraction and transmission electron microscopy, Mater. Charact. 147 (2019) 398–405.
[32] G.D. Ren, C.R. Dai, W. Mei, J. Sun, S. Lu, L. Vitos, Formation and temporal evolution of modulated structure in high Nb-containing lamellar γ-TiAl alloy, Acta Mater. 165 (2019) 215–227.
[33] M.W. Rackel, A. Stark, H. Gabrisch, F. Pyczak, Screening for O phase in advanced γ-TiAl alloys, Intermetallics 131 (2021) 107086.
[34] T.I. Nazarova, V.M. Imayev, R.M. Imayev, H.J. Fecht, Study of microstructure and mechanical properties of Ti-45Al-(Fe,Nb) (at.%) alloys, Intermetallics 82 (2017) 26–31.
[35] G.H. Cao, A.M. Russell, C.G. Oertel, W. Skrotzki, Microstructural evolution of TiAl-based alloys deformed by high-pressure torsion, Acta Mater. 98 (2015) 103–112.
[36] T. Schmoelzer, A. Stark, E. Schwaighofer, T. Lippmann, S. Mayer, H. Clemens, In situ synchrotron study of B19 phase formation in an intermetallic γ-TiAl alloy, Adv. Eng. Mater. 14 (7) (2012) 445–448.
[37] Y.H. Zhou, W.P. Li, D.W. Wang, L. Zhang, K. Ohara, J. Shen, T. Ebel, M. Yan, Selective laser melting enabled additive manufacturing of Ti-22Al-25Nb intermetallic: Excellent combination of strength and ductility, and unique microstructural features associated, Acta Mater. 173 (2019) 117–129.
[38] R. Hoppe, F. Appel, Deformation-induced internal stresses in multiphase titanium aluminide alloys, Acta Mater. 64 (2014) 169–178.
[39] B.G. Liu, L.H. Liu, W.D. Xing, R.C. Liu, R. Yang, P.A. Withey, J. Zhu, R. Yu, Structural stability and the alloying effect of TiB polymorphs in TiAl alloys, Intermetallics 90 (2017) 97–102.
[40] J. Li, S. Jeffs, M. Whittaker, N. Martin, Boride formation behaviour and their effect on tensile ductility in cast TiAl-based alloys, Mater. Des. 195 (2020) 109064.
[41] H.X. Li, X. Huang, L.C. Qi, C.X. Cao, Beneficial effects of boron addition into γ-TiAl alloys, Mater. Sci. Forum 539- 543 (2007) 1451–1456.
[42] J.C. Han, S.L. Xiao, J. Tian, Y.Y. Chen, L.J. Xu, X.P. Wang, Y. Jia, Z.X. Du, S.Z. Cao, Grain refinement by trace TiB_2 addition in conventional cast TiAl-based alloy, Mater. Charact. 106 (2015) 112–122.
[43] T.E.J. Edwards, F.D. Gioacchino, R. Muñoz-Moreno, W.J. Clegg, The interaction of borides and longitudinal twinning in polycrystalline TiAl alloys, Acta Mater. 140 (2017) 305–316.
[44] Y. Jia, Z.D. Liu, S. Li, H.M. Yao, Z.K. Ren, T. Wang, J.C. Han, S.L. Xiao, Y.Y. Chen, Effect of cooling rate on solidification microstructure and mechanical properties of TiB_2-containing TiAl alloy, T. Nonferrous Metal. Soc. 31 (2) (2021) 391–403.
[45] L. Wang, U. Lorenz, M. Münch, A. Stark, F. Pyczak, Influence of alloy composition and thermal history on carbide precipitation in γ-based TiAl alloys, Intermetallics 89 (2017) 32–39.
[46] L. Song, X.G. Hu, L. Wang, A. Stark, D. Lazurenko, U. Lorenz, J.P. Lin, F. Pyczak, T.B. Zhang, Microstructure evolution and enhanced creep property of a high Nb containing TiAl alloy with carbon addition, J. Alloy. Compd. 807 (2019) 151649.
[47] L. Wang, C. Zenk, A. Stark, P. Felfer, H. Gabrisch, M. Göken, U. Lorenz, F. Pyczak, Morphology evolution of Ti_3AlC carbide precipitates in high Nb containing TiAl alloys, Acta Mater. 137 (2017) 36–44.
[48] T. Klein, B. Rashkova, D. Holec, H. Clemens, S. Mayer, Silicon distribution and silicide precipitation during annealing in an advanced multi-phase γ-TiAl based alloy, Acta Mater. 110 (2016) 236–245.
[49] M.N. Mathabathe, A.S. Bolokang, G. Govender, R.J. Mostert, C.W. Siyasiya, Structure-property orientation relationship of a $\gamma/\alpha_2/Ti_5Si_3$ in as-cast Ti-45Al-2Nb-0.7Cr-0.3Si intermetallic alloy, J. Alloy. Compd. 765 (2018) 690–699.
[50] T. Liu, L.S. Luo, D.H. Zhang, L. Wang, X.Z. Li, R.R. Chen, Y.Q. Su, J.J. Guo, H.Z. Fu, Comparison of microstructures and mechanical properties of as-cast and directionally solidified Ti-47Al-1W-0.5Si alloy, J. Alloy. Compd. 682 (2016) 663–671.
[51] S. Bolz, M. Oehring, J. Lindemann, F. Pyczak, J. Paul, A. Stark, T. Lippmann, S. Schrüfer, D. Roth-Fagaraseanu, A. Schreyer, S. Weiß, Microstructure and mechanical properties of a forged β-solidifying γ TiAl alloy in different heat treatment conditions, Intermetallics 58 (2015) 71–83.
[52] K.F. Yao, H. Inui, K. Kishida, M. Yamaguchi, Plastic deformation of V- and Zr-alloyed PST TiAl in tension and compression at room temperature, Acta Metall. Mater. 43 (1995) 1075–1086.
[53] M.C. Kim, M.H. Oh, D.M. Wee, H. Inui, M. Yamaguchi, Microstructure and mechanical properties of a two-phase TiAl alloy containing Mo in single-, DS- and poly-crystalline forms, Mater. T. JIM 37 (1996) 1197–1203.
[54] R.M. Imayev, V.M. Imayev, M. Oehring, F. Appel, Microstructural evolution during hot working of Ti aluminide alloys: influence of phase constitution and initial casting texture, Metall. Mater. Trans. A 36 (2005) 859–867.
[55] E. Schwaighofer, H. Clemens, S. Mayer, J. Lindemann, J. Klose, W. Smarsly, V. Guether, Microstructural design and mechanical properties of a cast and heat-treated intermetallic multi-phase gamma-TiAl based alloy, Intermetallics 44 (2014) 128–140.
[56] D. Wimler, J. Lindemann, T. Kremmer, H. Clemens, S. Mayer, Microstructure and mechanical properties of novel TiAl alloys tailored via phase and precipitate morphology, Intermetallics 138 (2021) 107316.
[57] G.M. Zheng, B. Tang, S.K. Zhao, W.Y. Wang, X.F. Chen, L. Zhu, J.S. Li, Evading the strength-ductility trade-off at room temperature and achieving ultrahigh plasticity at 800°C in a TiAl alloy, Acta Mater. 225 (2022) 117585.
[58] T.L. Zhang, D. Wang, J.M. Zhu, H. Xiao, C.T. Liu, Y.Z. Wang, Non-conventional transformation pathways and ultrafine lamellar structures in γ-TiAl alloys, Acta Mater. 189 (2020) 25–34.

[59] H.G. Xiang, W.L. Guo, Synergistic effects of twin boundary and phase boundary for enhancing ultimate strength and ductility of lamellar TiAl single crystals, Int. J. Plast. 150 (2022) 103197.
[60] A. Neogi, R. Janisch, Twin-boundary assisted crack tip plasticity and toughening in lamellar γ-TiAl, Acta Mater. 213 (2021) 116924.
[61] M.J. Yan, F. Yang, H.T. Zhang, C.Z. Zhang, C.G. Chen, Z.M. Guo, Microstructure and mechanical properties of Co-containing Ti-48Al alloys prepared from irregular pre-alloyed powder, J. Alloy. Compd. 911 (2022) 165050.
[62] V. Singh, C. Mondal, R. Sarkar, P.P. Bhattacharjee, P. Ghosal, Effects of Cr alloying on the evolution of solidification microstructure and phase transformations of high-Nb containing γ-TiAl based alloys, Intermetallics 131 (2021) 107117.
[63] X.D. Wang, R.C. Luo, F. Liu, F. Zhu, S.X. Song, B. Chen, X.W. Zhang, J. Zhang, M.W. Chen, Characterization of Gd-rich precipitates in a fully lamellar TiAl alloy, Scr. Mater. 137 (2017) 50–54.
[64] Q. Wang, H.S. Ding, H.L. Zhang, R.R. Chen, J.J. Guo, H.Z. Fu, Influence of Mn addition on the microstructure and mechanical properties of a directionally solidified γ-TiAl alloy, Mater. Charact. 137 (2018) 133–141.
[65] H. Xu, X.B. Li, W.W. Xing, L. Shu, Y.C. Ma, K. Liu, Solidification pathway and phase transformation behavior in a beta-solidified gamma-TiAl based alloy, J. Mater. Sci. Technol. 35 (11) (2019) 2652–2657.
[66] N. Abdoshahi, M. Dehghani, L. Hatzenbichler, P. Spoerk-Erdely, A.V. Ruban, M. Musi, S. Mayer, J. Spitaler, D. Holec, Structural stability and mechanical properties of TiAl+Mo alloys: a comprehensive ab initio study, Acta Mater. 221 (2021) 117427.
[67] Z.T. Gao, R. Hu, Z.J. Huang, Y.L. Wu, J.G. Li, M. Zhou, Metastable transformation behavior in a Ta-containing TiAl-Nb, Alloy. Contin. Cool., J. Alloy. Compd. 904 (2022) 164088.
[68] X.B. Li, H.J. Tang, W.W. Xing, P.X. Zhao, B. Chen, Y.C. Ma, K. Liu, Microstructural stability, phase evolution and mechanical properties of a forged W-modified high-Mn β-γ-TiAl alloy, Intermetallics 136 (2021) 107230.
[69] X.S. Xu, H.S. Ding, H.T. Huang, H. Liang, R.R. Chen, J.J. Guo, H.Z. Fu, Effect of V on the microstructure and brittle-to-ductile transition of directionally solidified high-Nb TiAl alloy, Intermetallics 142 (2022) 107455.
[70] X. Gu, S.D. Jiang, F.Y. Cao, G.Q. Zhang, D.Y. Yang, S. Guo, H.Q. Song, J.F. Sun, A. β-solidifying, TiAl alloy reinforced with ultra-fine Y-rich precipitates, Scr. Mater. 192 (2021) 55–60.
[71] V.M. Imayev, A.A. Ganeev, D.M. Trofimov, N.J. Parkhimovich, R.M. Imayev, Effect of Nb, Zr and Zr + Hf on the microstructure and mechanical properties of β-solidifying γ-TiAl alloys, Mater. Sci. Eng. A 817 (2021) 141388.
[72] T. Klein, M. Schachermayer, F. Mendez-Martin, T. Schöberl, B. Rashkova, H. Clemens, S. Mayer, Carbon distribution in multi-phase γ-TiAl based alloys and its influence on mechanical properties and phase formation, Acta Mater. 94 (2015) 205–213.
[73] H.Z. Fang, S. Wang, R.R. Chen, Q. Xu, Y.D. Yan, Y.Q. Su, J.J. Guo, The effects of the formation of a multi-scale reinforcing phase on the microstructure evolution and mechanical properties of a Ti_2AlC/TiAl alloy, Nanoscale 13 (29) (2021) 12565–12576.
[74] S. Yim, H.K. Bian, K. Aoyagi, A. Chiba, Effect of multi-stage heat treatment on mechanical properties and microstructure transformation of Ti-48Al-2Cr-2Nb alloy, Mater. Sci. Eng. A 816 (2021) 141321.
[75] G. Yang, H.C. Kou, J.R. Yang, J.S. Li, H.Z. Fu, Microstructure control of Ti-45Al-8.5Nb(W, B, Y) alloy during the solidification process, Acta Mater. 112 (2016) 121–131.
[76] S.Q. Liu, H.S. Ding, R.R. Chen, J.J. Guo, H.Z. Fu, Remarkable improvement in tensile strength of a polycrystalline γ-TiAl based intermetallic alloy by deformation nanotwins, Mater. Sci. Eng. A 823 (2021) 141692.
[77] R.R. Xu, H. Li, M.Q. Li, Dynamic recrystallization mechanism of gamma and alpha phases during the isothermal compression of gamma-Al alloy with duplex structure, J. Alloy. Compd. 844 (2020) 156089.
[78] R.R. Xu, M.Q. Li, Quantitative characterization of β-solidifying γ-TiAl alloy with duplex structure, T. Nonferrous Metal. Soc. 31 (7) (2021) 1993–2004.
[79] R.R. Xu, M.Q. Li, Deformability of β phase in Ti-42.9Al-4.6Nb-2Cr, J. Alloy. Compd. 871 (2021) 159617.
[80] Z.X. Chen, H.S. Ding, R.R. Chen, S.Q. Liu, J.J. Guo, H.Z. Fu, An innovative method for the microstructural modification of TiAl alloy solidified via direct electric current application, J. Mater. Sci. Technol. 35 (1) (2019) 23–28.
[81] R.R. Chen, D.S. Zheng, T.F. Ma, H.S. Ding, Y.Q. Su, J.J. Guo, H.Z. Fu, Effects and mechanism of ultrasonic irradiation on solidification microstructure and mechanical properties of binary TiAl alloys, Ultrason. Sonochem. 38 (2017) 120–133.
[82] H.L. Zhu, M.J. Qin, R. Aughterson, T. Wei, G. Lumpkin, Y. Ma, H.J. Li, Atomic origins of radiation-induced defects and the role of lamellar interfaces in radiation damage of titanium aluminide alloy irradiated with Kr-ions at elevated temperature, Acta Mater. 172 (2019) 72–83.
[83] H.L. Zhu, M.J. Qin, R. Aughterson, T. Wei, G. Lumpkin, Y. Ma, H.J. Li, The formation and accumulation of radiation-induced defects and the role of lamellar interfaces in radiation damage of titanium aluminum alloy irradiated with Kr-ions at room temperature, Acta Mater. 195 (2020) 654–667.
[84] L.E. Murr, S.M. Gaytan, A. Ceylan, E. Martinez, J.L. Martinez, D.H. Hernandez, B.I. Machado, D.A. Ramirez, F. Medina, S. Collins, R.B. Wicker, Characterization of titanium aluminide alloy components fabricated by additive manufacturing using electron beam melting, Acta Mater. 58 (5) (2010) 1887–1894.
[85] T.H. Becker, P. Kumar, U. Ramamurty, Fracture and fatigue in additively manufactured metals, Acta Mater. 219 (2021) 117240.
[86] ⟨https://www.geaviation.com/propulsion/commercial/ge9x⟩, (accessed 09. 10.22).
[87] D. Huang, Q.Y. Tan, Y.H. Zhou, Y. Yin, F. Wang, T. Wu, X.L. Yang, Z.Q. Fan, Y.G. Liu, J.Q. Zhang, H. Huang, M. Yan, M.X. Zhang, The significant impact of grain refiner on γ-TiAl intermetallic fabricated by laser-based additive manufacturing, Addit. Manuf. 46 (2021) 102172.
[88] C. Guo, G. Li, S. Li, X.G. Hu, H.X. Lu, X.G. Li, Z. Xu, Y.H. Chen, Q.Q. Li, J. Lu, Q. Zhu, Additive manufacturing of Ni-based superalloys: residual stress, mechanisms of crack formation and strategies for crack inhibition, Nano Mater. Sci. (2022).
[89] P. Kontis, E. Chauvet, Z.R. Peng, J.Y. He, A.K.D. Silva, D. Raabe, C. Tassin, J.-J. Blandin, S. Abed, R. Dendievel, B. Gault, G. Martin, Atomic-scale grain boundary engineering to overcome hot-cracking in additively-manufactured superalloys, Acta Mater. 177 (2019) 209–221.
[90] M.S. Wang, E.W. Liu, Y.L. Du, T.T. Liu, W.H. Liao, Cracking mechanism and a novel strategy to eliminate cracks in TiAl alloy additively manufactured by selective laser melting, Scr. Mater. 204 (2021) 114151.
[91] M. Todai, T. Nakano, T. Liu, H.Y. Yasuda, K. Hagihara, K. Cho, M. Ueda, M. Takeyama, Effect of building direction on the microstructure and tensile properties of Ti-48Al-2Cr-2Nb alloy additively manufactured by electron beam melting, Addit. Manuf. 13 (2017) 61–70.
[92] Y. Ma, D. Cuiuri, C. Shen, H.J. Li, Z.X. Pan, Effect of interpass temperature on in-situ alloying and additive manufacturing of titanium aluminides using gas tungsten arc welding, Addit. Manuf. 8 (2015) 71–77.
[93] K. Cho, H. Kawabata, T. Hayashi, H.Y. Yasuda, H. Nakashima, M. Takeyama, T. Nakano, Peculiar microstructural evolution and tensile properties of β-containing γ-TiAl alloys fabricated by electron beam melting, Addit. Manuf. 46 (2021) 102091.
[94] Z.Q. Liu, C.Y. Wang, W.B. Wang, G.J. Xu, X.Y. Liu, Effects of Tantalum on the microstructure and properties of Ti-48Al-2Cr-2Nb alloy fabricated via laser additive manufacturing, Mater. Charact. 179 (2021) 111317.
[95] H.Y. Yue, H. Peng, R.F. Li, R.Q. Gao, X.P. Wang, Y.Y. Chen, High-temperature microstructure stability and fracture toughness of TiAl alloy prepared via electron beam smelting and selective electron beam melting, Intermetallics 136 (2021) 107259.
[96] Y. Ma, D. Cuiuri, H.J. Li, Z.X. Pan, C. Shen, The effect of postproduction heat treatment on γ-TiAl alloys produced by the GTAW-based additive manufacturing process, Mater. Sci. Eng. A 657 (2016) 86–95.
[97] D. Wimler, K. Käsznar, M. Musi, C. Breuning, M. Markl, J. Keckes, H. Clemens, C. Körner, S. Mayer, How electron beam melting tailors the Al-sensitive microstructure and mechanical response of a novel process-adapted γ-TiAl based alloy, Mater. Des. 212 (2021) 110187.
[98] X.Y. Zhang, C.W. Li, M.H. Wu, Z.H. Ye, Q. Wang, J.F. Gu, Atypical pathways for lamellar and twinning transformations in rapidly solidified TiAl alloy, Acta Mater. 227 (2022) 117718.
[99] H.L. Zhu, Y. Ma, T. Wei, H.J. Li, R. Aughterson, G. Lumpkin, The formation and Kr-ion irradiation behaviour of new microstructural features in additively manufactured titanium aluminium alloy, Addit. Manuf. 29 (2019) 100766.
[100] C. Stangl, E. Kollmannsberger, T.A. Zimogliadova, M. Krüger, H. Saage, Influence of a fine-grained surface structure on the tensile behaviour of a beta stabilised intermetallic γ-TiAl-based alloy, Intermetallics 146 (2022) 107566.
[101] A. Gaitzenauer, A. Stark, D. Gosslar, H. Clemens, S. Mayer, Microstructure and texture evolution in an intermetallic β-stabilized TiAl alloy during forging and subsequent isothermal annealing, Adv. Eng. Mater. 16 (4) (2014) 445–451.
[102] D.S. Wen, S.H. Huang, B. Guo, D.B. Shan, Y.Y. Zong, Effect of hydrogen on γ−phase transformation and texture evolution of a TiAl-based alloy deformed at elevated temperature, Mater. Sci. Eng. A 699 (2017) 176–184.
[103] Y. Zhang, X.P. Wang, F.T. Kong, L.L. Sun, Y.Y. Chen, Microstructure, texture and mechanical properties of Ti-43Al-9V-0.2Y alloy hot-rolled at various temperatures, J. Alloy. Compd. 777 (2019) 795–805.
[104] Q.B. Wang, S.Z. Zhang, C.J. Zhang, Z.W. Song, D.D. Zhu, D. Dong, S.L. Zhang, Effect of hot rolling temperature on microstructure evolution, deformation texture and nanoindentation properties of an intermetallic Ti-43Al-9V-0.2Y alloy, Intermetallics 117 (2020) 106677.
[105] P. Erdely, P. Staron, E. Maawad, N. Schell, J. Klose, H. Clemens, S. Mayer, Design and control of microstructure and texture by thermomechanical processing of a multi-phase TiAl alloy, Mater. Des. 131 (2017) 286–296.
[106] P. Erdely, P. Staron, E. Maawad, N. Schell, J. Klose, S. Mayer, H. Clemens, Effect of hot rolling and primary annealing on the microstructure and texture of a β-stabilised γ-TiAl based alloy, Acta Mater. 126 (2017) 145–153.
[107] H.Y. Yue, Y.Y. Chen, X.P. Wang, S.L. Xiao, F.T. Kong, Microstructure, texture and tensile properties of Ti-47Al-2Cr-2Nb alloy produced by selective electron beam melting, J. Alloy. Compd. 766 (2018) 450–459.
[108] Z.Q. Liu, G.L. Yin, X.O. Zhu, Q. Zhou, Microstructure, texture and tensile properties as a function of laser power of Ti-48Al-2Cr-2Nb-5Ta alloy prepared by laser additive manufacturing, J. Manuf. Process. 73 (2022) 624–632.
[109] Y.L. Hao, D.S. Xu, Y.Y. Cui, R. Yang, D. Li, The site occupancies of alloying elements in TiAl and Ti_3Al alloys, Acta Mater. 47 (4) (1999) 1129–1139.

[110] A. Stark, M. Oehring, F. Pyczak, A. Schreyer, In situ observation of various phase transformation paths in Nb-rich TiAl alloys during quenching with different rates, Adv. Eng. Mater. 13 (8) (2011) 700–704.
[111] R.R. Xu, H. Li, M.Q. Li, Flow softening mechanism in isothermal compression of β-solidifying γ-TiAl alloy, Mater. Des. 186 (2020) 108328.
[112] R.R. Xu, M.Q. Li, H. Li, Kinetic analysis and strain-compensated constitutive models of Ti-42.9Al-4.6Nb-2Cr during isothermal compression, Prog. Nat. Sci. Mater. 30 (2) (2020) 260–269.
[113] Y. Pan, X. Lu, C.C. Liu, T.L. Hui, C. Zhang, X.H. Qu, Sintering densification, microstructure and mechanical properties of Sn-doped high Nb-containing TiAl alloys fabricated by pressureless sintering, Intermetallics 125 (2020) 106891.
[114] H.Y. Yue, Y.Y. Chen, X.P. Wang, F.T. Kong, Effect of beam current on microstructure, phase, grain characteristic and mechanical properties of Ti-47Al-2Cr-2Nb alloy fabricated by selective electron beam melting, J. Alloy. Compd. 750 (2018) 617–625.
[115] W.J. Zhang, F. Appel, Effect of Al content and Nb addition on the strength and fault energy of TiAl alloys, Mater. Sci. Eng. A 329–331 (2002) 649–652.
[116] J.Y. Kim, E.S. Park, T. Lee, S. Ryu, S.-E. Kim, S.-W. Kim, Origin of enhanced room temperature ductility in TiAl alloys: reducing activation difference of deformation mechanism of γ phase, J. Alloy. Compd. 899 (2022) 163307.
[117] J.C. Han, J. Dong, S.Z. Zhang, C.J. Zhang, S.L. Xiao, Y.Y. Chen, Microstructure evolution and tensile properties of conventional cast TiAl-based alloy with trace Ni addition, Mater. Sci. Eng. A 715 (2018) 41–48.
[118] Q. Wang, H.S. Ding, H.L. Zhang, R.R. Chen, J.J. Guo, H.Z. Fu, Variations of microstructure and tensile property of γ-TiAl alloys with 0-0.5 at.% C additives, Mater. Sci. Eng. A 700 (2017) 198–208.
[119] W. Li, M. Li, J. Liu, Y. Yang, D.S. Cai, Q.S. Wei, C.Z. Yan, Y.S. Shi, Microstructures and mechanical properties of nano-WC reinforced Ti-44.5Al-5Nb-0.5W-0.5C-0.2B alloy prepared by hot isostatic pressing, J. Alloy. Compd. 770 (2019) 640–648.
[120] S.L. Xiao, Y.F. Guo, Z.Q. Liang, X.N. Wang, J.K. Yang, X. Wang, L.J. Xu, J. Tian, Y.Y. Chen, The effect of nano-Y_2O_3 addition on tensile properties and creep behavior of as-cast TiAl alloy, J. Alloy. Compd. 825 (2020) 153852.
[121] X.S. Xu, H.S. Ding, H.T. Huang, H. Liang, R.R. Chen, J.J. Guo, H.Z. Fu, Microstructure and elevated temperature tensile property of Ti-46Al-7Nb-(W,Cr,B) alloy compared with binary and ternary TiAl alloy, Mater. Sci. Eng. A 807 (2021) 140902.
[122] S.L. Xiao, Z.Q. Liang, Y.F. Zheng, H. Zhao, Y.F. Guo, L.J. Xu, X. Xue, J. Tian, Y.Y. Chen, The tensile creep behavior of a B_4C-bearing high Nb containing TiAl alloy, Intermetallics 141 (2022) 107410.
[123] L. Chen, L.P. Zhu, Y.J. Guan, B. Zhang, J.C. Li, Tougher TiAl alloy via integration of hot isostatic pressing and heat treatment, Mater. Sci. Eng. A 688 (2017) 371–377.
[124] Y.Z. Wang, W. Li, H. Yuan, H.S. Ding, R.R. Chen, J.J. Guo, H.Z. Fu, Microstructure refinement and improvement of mechanical properties of Ti-46Al-8Nb-0.9B alloys by electromagnetic cold crucible continuous solidification, Intermetallics 140 (2022) 107391.
[125] X.A. Yue, J. Shen, Y.L. Xiong, S.K. Zheng, Microstructure control and mechanical properties of directionally solidified large size TiAl alloy by electromagnetic confinement, Intermetallics 140 (2022) 107406.
[126] Z.Z. Xia, Y.Y. Cui, Y.Y. Shen, M. Arroussi, R.H. Liu, L. Yang, Q. Jia, R. Yang, Tensile properties of Ti-48Al-2Cr-2Nb alloy having similarly oriented lamellae with fine lamellar spacing facilitated by suction casting, Mater. Sci. Eng. A 830 (2022) 142303.
[127] R.R. Chen, Y.L. Liu, X. Xue, H.Z. Fang, Y.M. Tan, H.Z. Cui, Study on improving microstructure and mechanical properties of directionally solidified Ti-44Al-6Nb-1Cr alloy by cyclic DHT, Mater. Sci. Eng. A 809 (2021) 140912.
[128] R. Hu, Y.L. Wu, J.R. Yang, Z.T. Gao, J.G. Li, Phase transformation pathway and microstructural refinement by feathery transformation of Ru-containing γ-TiAl alloy, J. Mater. Res. Technol. 18 (2022) 5290–5300.
[129] A. Couret, D. Reyes, M. Thomas, N. Ratel-Ramond, C. Deshayes, J.-P. Monchoux, Effect of ageing on the properties of the W-containing IRIS-TiAl alloy, Acta Mater. 199 (2020) 169–180.
[130] H.W. Liu, Z.X. Li, F. Gao, Y.G. Liu, Q.F. Wang, High tensile ductility and strength in the Ti-42Al-6V–1Cr alloy, J. Alloy. Compd. 698 (2017) 898–905.
[131] E.T. Zhao, H.Z. Niu, S.Z. Zhang, L. Feng, S.Y. Yang, Microstructural control and mechanical properties of a β-solidified γ-TiAl alloy Ti-46Al-2Nb-1.5V–1Mo-Y, Mater. Sci. Eng. A 701 (2017) 1–6.
[132] W.C. Xu, X.Z. Jin, K. Huang, Y.Y. Zong, S.F. Wu, X.M. Zhong, F.T. Kong, D.B. Shan, S. Nutt, Improvement of microstructure, mechanical properties and hot workability of a TiAl-Nb-Mo alloy through hot extrusion, Mater. Sci. Eng. A 705 (2017) 200–209.
[133] Z.Q. Liu, R.X. Ma, G.J. Xu, W.B. Wang, Y.H. Su, Effects of annealing on microstructure and mechanical properties of γ-TiAl alloy fabricated via laser melting deposition, T. Nonferous Metal. Soc. 30 (4) (2020) 917–927.
[134] J. Pelleg, Mechanical Properties of Materials, Springer, Dordrecht, Netherlands, 2013, pp. 259–337.
[135] A. Couret, J.-P. Monchoux, D. Caillard, On the high creep strength of the W containing IRIS-TiAl alloy at 850 °C, Acta Mater. 181 (2019) 331–341.
[136] J. Lapin, T. Pelachová, O. Bajana, High temperature deformation behaviour and microstructure of cast in-situ TiAl matrix composite reinforced with carbide particles, J. Alloy. Compd. 797 (2019) 754–765.
[137] Y.F. Guo, J. Tian, S.L. Xiao, L.J. Xu, Y.Y. Chen, Enhanced creep properties of Y_2O_3-bearing Ti-48Al-2Cr-2Nb alloys, Mater. Sci. Eng. A 809 (2021) 140952.
[138] S.K. Zhang, S.G. Tian, G.Y. Li, N. Tian, F.W. Jin, H.C. Yu, X.X. Lv, G.Y. Wang, D.Y. Li, Creep behavior and effect factors of a TiAl-Nb alloy at high temperature, Prog. Nat. Sci. Mater. 31 (3) (2021) 477–485.
[139] Y.C. Wang, X.Y. Xue, H.C. Kou, Y.H. Yu, M.Y. Jia, J.S. Li, The interfacial β_0 phase strengthening the creep properties of powder hot isostatic pressing γ-TiAl alloy, Mater. Res. Lett. 10 (5) (2022) 327–333.
[140] J. Ding, S.T. Huang, Z.L. Dong, J.P. Lin, Y. Ren, X.D. Wu, H. Chang, Thermal stability and lattice strain evolution of high Nb-containing TiAl alloy under low-cycle fatigue loading, Adv. Eng. Mater. 23 (9) (2021) 2001337.
[141] J. Ding, Y.F. Liang, X.J. Xu, H.C. Yu, C.L. Dong, J.P. Lin, Cyclic deformation and microstructure evolution of high Nb-containing TiAl alloy during high temperature low cycle fatigue, Int. J. Fatigue 99 (2017) 68–77.
[142] J. Ding, M.Z. Zhang, T. Ye, Y.F. Liang, Y. Ren, C.L. Dong, J.P. Lin, Microstructure stability and micro-mechanical behavior of as-cast gamma-TiAl alloy during high-temperature low cycle fatigue, Acta Mater. 145 (2018) 504–515.
[143] K. Cho, R. Kobayashi, J.Y. Oh, H.Y. Yasuda, M. Todai, T. Nakano, A. Ikeda, M. Ueda, M. Takeyama, Influence of unique layered microstructure on fatigue properties of Ti-48Al-2Cr-2Nb alloys fabricated by electron beam melting, Intermetallics 95 (2018) 1–10.
[144] C.L. Dong, Z.H. Jiao, H.C. Yu, H.T. Zhou, F.T. Kong, Y.Y. Chen, Effect of dwell condition on fatigue behavior of a high-Nb TiAl alloy at 750°C, Intermetallics 91 (2017) 1–7.
[145] C.L. Dong, H.C. Yu, Z.H. Jiao, F.T. Kong, Y.Y. Chen, Low cycle fatigue, creep and creep-fatigue interaction behavior of a TiAl alloy at high temperatures, Scr. Mater. 144 (2018) 60–63.
[146] C. Löffl, H. Saage, M. Göken, The influence of near service environmental conditions on the corrosion and LCF behaviour of a beta-stabilized γ-TiAl alloy, Corros. Sci. 175 (2020) 108885.
[147] Q. Zhang, X.A. Hu, Z.R. Zhang, T. Sun, J.W. Wu, Y.F. Li, T.T. Ren, The mean stress and phase angle effect on multiaxial fatigue behavior of a TiAl alloy: failure analysis and life modeling, Int. J. Mech. Sci. 193 (2021) 106123.
[148] Z.W. Huang, J.P. Lin, B. Feng, Microstructural characterization and fatigue response of alloy Ti-46Al-5Nb-1W with varied surface quality and thermal exposure history, Mater. Charact. 130 (2017) 285–297.
[149] T.E.J. Edwards, F.D. Gioacchino, A.J. Goodfellow, W.J. Clegg, Slip bands in lamellar TiAl during high cycle fatigue microcompression by correlative total strain mapping, diffraction orientation mapping and transmission electron imaging, Int. J. Fatigue 124 (2019) 520–527.
[150] X.S. Xu, H.S. Ding, W. Li, H.T. Huang, H. Liang, S. Kwak, R.R. Chen, J.J. Guo, H.Z. Fu, The smooth and notched three-point bending fatigue behavior of directionally solidified high-Nb TiAl alloy, Mater. Charact. 181 (2021) 111444.
[151] Y. Chen, Y.D. Cao, Z.X. Qi, G. Chen, Increasing high-temperature fatigue resistance of polysynthetic twinned TiAl single crystal by plastic strain delocalization, J. Mater. Sci. Technol. 93 (2021) 53–59.
[152] X.S. Xu, H.S. Ding, W. Li, H.T. Huang, H. Liang, R.R. Chen, J.J. Guo, H.Z. Fu, The microstructure and high cycle fatigue performance of as-cast and directionally solidified Ti-46Al-7Nb alloy under the three-point bending loading, Mater. Sci. Eng. A 822 (2021) 141633.
[153] C.F. Yao, J.N. Lin, D.X. Wu, J.X. Ren, Surface integrity and fatigue behavior when turning γ-TiAl alloy with optimized PVD-coated carbide inserts, Chin. J. Aeronaut. 31 (4) (2018) 826–836.
[154] P. Sallot, J.P. Monchoux, S. Joulié, A. Couret, M. Thomas, Impact of β-phase in TiAl alloys on mechanical properties after high temperature air exposure, Intermetallics 119 (2020) 106729.
[155] Y.L. Yang, C.L. Wang, Y.Z. Gesang, H.F. Shang, R. Wang, Y.M. Liang, T.C. Wang, Q. Chen, T.M. Shao, Fretting wear evolution of γ-TiAl alloy, Tribol. Int. 154 (2021) 106721.
[156] J. Cheng, Y. Yu, L.C. Fu, F. Li, Z.H. Qiao, J.S. Li, J. Yang, W.M. Liu, Effect of TiB_2 on dry-sliding tribological properties of TiAl intermetallics, Tribol. Int. 62 (2013) 91–99.
[157] H.L. Wang, Q. Wang, L.C. Zeng, H.L. Zhang, H.S. Ding, Microstructure, mechanical and tribological performances of a directionally solidified γ-TiAl alloy, Mater. Charact. 179 (2021) 111393.
[158] L. Mengis, C. Grimme, M.C. Galetz, High-temperature sliding wear behavior of an intermetallic γ-based TiAl alloy, Wear 426–427 (2019) 341–347.
[159] A. Ismaeel, C.S. Wang, Effect of Nb additions on microstructure and properties of γ-TiAl based alloys fabricated by selective laser melting, T. Nonferrous Metal. Soc. 29 (5) (2019) 1007–1016.
[160] K. Hua, Q. Wan, Y.L. Tong, G. Yang, H.X. Wu, Q. Zhou, H.F. Wang, Microstructural feature dependence of dry sliding wear behaviors in a γ-TiAl alloy, Wear 484-485 (2021) 204039.
[161] J. Cheng, S.Y. Zhu, Y. Yu, J. Yang, W.M. Liu, Microstructure, mechanical and tribological properties of TiAl-based composites reinforced with high volume fraction of nearly network Ti_2AlC particulates, J. Mater. Sci. Technol. 34 (4) (2018) 670–678.

[162] J.W. Qiu, Z.F. Fu, B. Liu, Y. Liu, J.H. Yan, D. Pan, W.D. Zhang, I. Baker, Effects of niobium particles on the wear behavior of powder metallurgical γ-TiAl alloy in different environments, Wear 434–435 (2019) 202964.
[163] J.W. Qiu, Z.F. Fu, B. Liu, Y. Liu, J.H. Yan, D. Pan, W.D. Zhang, Wear behavior of P/M high Nb containing γ-TiAl alloy in different environments, Met. Mater. Int. 25 (6) (2019) 1564–1573.
[164] J. Cheng, F. Li, S.Y. Zhu, Y. Yu, Z.H. Qiao, J. Yang, Electrochemical corrosion and tribological evaluation of TiAl alloy for marine application, Tribol. Int. 115 (2017) 483–492.
[165] A. Raina, Volume dependent fracture energy and brittle to quasi-brittle transition in intermetallic alloys, Eng. Fract. Mech. 264 (2022) 108312.
[166] A. Neogi, R. Janisch, Unravelling the lamellar size-dependent fracture behavior of fully lamellar intermetallic γ-TiAl, Acta Mater. 227 (2022) 117698.
[167] Y.Z. Wang, H. Yuan, H.S. Ding, R.R. Chen, J.J. Guo, H.Z. Fu, W. Li, Effects of lamellar orientation on the fracture toughness of TiAl PST crystals, Mater. Sci. Eng. A 752 (2019) 199–205.
[168] B. Zhu, X.Y. Xue, H.C. Kou, X.L. Li, J.S. Li, Effect of microstructure on the fracture toughness of multi-phase high Nb-containing TiAl alloys, Intermetallics 100 (2018) 142–150.
[169] A. Lintner, R. Pippan, M. Schloffer, A. Hohenwarter, Effect of a single overload on the cyclic R-curve behaviour of a γ-TiAl TNM alloy, Int. J. Fatigue 163 (2022) 107083.
[170] G. Molénat, B. Galy, M. Musi, L. Toualbi, M. Thomas, H. Clemens, J.-P. Monchoux, A. Couret, Plasticity and brittleness of the ordered βo phase in a TNM-TiAl alloy, Intermetallics 151 (2022) 107653.
[171] F. Appel, J.D.H. Paul, P. Staron, M. Oehring, O. Kolednik, J. Predan, F.D. Fischer, The effect of residual stresses and strain reversal on the fracture toughness of TiAl alloys, Mater. Sci. Eng. A 709 (2018) 17–29.
[172] S.K. Zhang, N. Tian, D.Y. Li, J.H. Li, F.W. Jin, G.Y. Wang, S.G. Tian, Microstructure evolution and fracture mechanism of a TiAl-Nb alloy during high-temperature tensile testing, Mater. Sci. Eng. A 831 (2022) 142094.